9-2021

A Mélange of Subduction Ages: Constraints on the Timescale of Shear Zone Development and Underplating at the Subduction Interface, Catalina Schist (CA, USA)

K. M. Harvey
University of Maryland

S. Walker
Boston College

P. G. Starr
Boston College

S. C. Penniston-Dorland
University of Maryland

M. J. Kohn
Boise State University

See next page for additional authors

Geochemistry, Geophysics, Geosystems®

RESEARCH ARTICLE
10.1029/2021GC009790

Special Section:
Insights into Subduction Zone Processes from Models and Observations of Exhumed Terranes

A Mélange of Subduction Ages: Constraints on the Timescale of Shear Zone Development and Underplating at the Subduction Interface, Catalina Schist (CA, USA)

K. M. Harvey[1,2], S. Walker[2,3], P. G. Starr[2], S. C. Penniston-Dorland[1], M. J. Kohn[4], and E. F. Baxter[2]

[1]Department of Geology, University of Maryland, College Park, MD, USA, [2]Department of Earth and Environmental Sciences, Boston College, Chestnut Hill, MA, USA, [3]Center for Isotope Geochemistry, Boston College, Chestnut Hill, MA, USA, [4]Department of Geosciences, Boise State University, Boise, ID, USA

Abstract The presence of mélange at the subduction interface influences numerous geochemical and geophysical processes. However, the relationship between the timescales of mélange development, deformation, and resultant mass transport is poorly understood. Here, we use Sm-Nd garnet geochronology to elucidate the timing of peak metamorphism for five garnet amphibolite tectonic blocks from the amphibolite-facies mélange zone of the Catalina Schist (Santa Catalina Island, CA). Ages range from 108 to 116 Ma and do not appear to correlate with the peak metamorphic temperature recorded by each block (between 640 and 740°C). The lack of correlation between age and peak temperature favors the tectonic mixing model previously proposed for the unit. These ages overlap with previous estimates of 111–114 Ma for peak metamorphism of the mélange zone but are predominately younger than an estimate for the structurally lower coherent amphibolite unit of ca. 115 Ma. White mica $^{40}Ar/^{39}Ar$ ages from previous studies suggest that the units cooled asynchronously to 400–425°C by 106 to 97 Ma at rates between 18 and 43°C/Ma. Collectively, these results demonstrate that mélange formation occurred over at least 8 Myr from 116 to 108 Ma and was followed by cooling. The structural and chronologic relationship between the mélange zone and underlying lower-grade units indicates that the cooling occurred in conjunction with an underplating event between 109 and 108 Ma. The age discrepancy between the mélange zone and the underlying coherent amphibolite unit may indicate that the two units were juxtaposed either during or after the underplating event.

Plain Language Summary The amphibolite-facies mélange zone of the Catalina Schist (Santa Catalina Island, CA) contains relatively rigid cm- to 100 m-scale blocks are encapsulated within a deformed and hydrated matrix, and is interpreted to represent a paleo-subduction interface between the Farallon and North American plates during a Cretaceous subduction event. The mélange zone is well-known for its preservation of subduction processes, including evidence for mechanical and geochemical mixing between the downgoing slab and overriding plate and pristine examples of fluid-rock interactions and melt generation. However, the timescale over which these processes occurred has been only loosely constrained. In this study, we utilize Sm-Nd garnet geochronology to directly date when blocks within the mélange approached their maximum depth prior to exhumation. Ages for five blocks range from 108 to 116 million years old, indicating that the mélange zone formed by progressive tectonic mixing over at least ca. 8 million years. We compare these ages to other chronologic constraints and show that the mélange zone and underlying coherent unit were underplated to the overriding plate between 109 and 108 million years ago. As a result of underplating, a new subduction interface formed beneath both units, terminating deformation and fluid transport within the mélange zone.

Key Points:

- Sm-Nd garnet geochronology was used to assess variations in peak age within the amphibolite-facies mélange zone of the Catalina Schist
- Rocks recording disparate peak temperatures and ages were juxtaposed between 116 and 108 Ma by mélange flow at the subduction interface
- The mélange zone and underlying coherent unit were underplated and rapidly cooled between 109 and 108 Ma

Supporting Information:

Supporting Information may be found in the online version of this article.

Correspondence to:

K. M. Harvey,
harveykf@bc.edu

Citation:

Harvey, K. M., Walker, S., Starr, P. G., Penniston-Dorland, S. C., Kohn, M. J., & Baxter, E. F. (2021). A mélange of subduction ages: Constraints on the timescale of shear zone development and underplating at the subduction interface, Catalina Schist (CA, USA). *Geochemistry, Geophysics, Geosystems*, *22*, e2021GC009790. https://doi.org/10.1029/2021GC009790

Received 16 MAR 2021
Accepted 2 SEP 2021

1. Introduction

Mélange at the subduction interface controls many important physico-chemical processes, including mass transfer between the downgoing slab and overriding plate, large-scale channelization of fluids, and the rheologic evolution of the plate interface. Both fluid transport at the subduction interface and the mechanical behavior of rigid blocks within a deforming matrix have recently been proposed to catalyze seismic phenomena occurring below the megathrust including episodic tremor and slip (ETS; e.g., Audet & Bürg-

mann, 2014; Beall et al., 2019; Behr & Bürgmann, 2021; French & Zhu, 2017; Kirkpatrick et al., 2021; Tarling et al., 2019), which occurs at depths between ~30 and 50 km. Understanding the controlling factors on the formation and evolution of mélange will help elucidate how feedbacks between metamorphism, deformation and fluid release at the subduction interface contribute to the seismic cycle and the dynamic evolution of subduction zones. Field-based observations in paleo-subduction terranes are particularly important for understanding how variations in controlling factors such as composition, thermal structure, and timescales of deformation influence the mechanical behavior of the subduction interface.

While subduction-related mélange can form by both tectonic and sedimentary processes, tectonic mélanges such as is found in the Catalina Schist are thought to develop by feedbacks among mechanical mixing, metasomatism and progressive metamorphism, whereby cm- to m-scale blocks sourced from the downgoing slab and overriding plate are mechanically incorporated into a fine-grained metasomatic matrix (e.g., Bebout & Penniston-Dorland, 2016). Metasomatism of these blocks drives the formation of hydrated reaction rinds, which can be mechanically ablated and incorporated into the matrix (e.g., Penniston-Dorland et al., 2014), creating a unique matrix composition that is geochemically and isotopically distinct from its end-member components (Bebout & Barton, 2002; King et al., 2006, 2007). Geochemical, petrologic and geodynamic evidence suggests that tectonic mélange development occurs throughout prograde and peak metamorphism (e.g., Gerya et al., 2002; Penniston-Dorland et al., 2014), as shearing between mélange components mixes materials of disparate lithologies and metamorphic grade.

The Catalina Schist amphibolite-facies mélange zone provides an opportunity to understand the relationship between spatial and temporal scales of tectonic mélange development and mixing at depths relevant to ETS. Blocks and matrix throughout the mélange zone all record amphibolite-facies metamorphic conditions with resolvable (up to 90°C; Penniston-Dorland et al., 2018) differences in peak metamorphic temperature. The spatial distribution of these temperatures throughout the zone is non-systematic and suggests that the material was mixed through a combination of metasomatism and localized deformation at the subduction interface. Interestingly, the scale of mixing based on this temperature disparity is small relative to other exhumed subduction-related mélange zones. For example, regions of the Franciscan Complex (northern California) and the Rio San Juan Complex (Dominican Republic) record up to ~400°C differences in peak metamorphic temperature among blocks (e.g., Krebs et al., 2011; Krohe, 2017; Tsujimori et al., 2006). Currently, there is little understanding of how the spatial scale of mixing is controlled by factors such as matrix rheology and the timescales over which mélange zones develops. Penniston-Dorland et al. (2018) related limited scales of mixing in the Catalina Schist to development of rheologically strong phases in the matrix, such as amphibole and pyroxene, as a result of prograde metamorphism. Their interpretation is supported by geodynamic models that demonstrate that rheologically weak matrix minerals permit larger scales of mixing than strong matrix minerals (Gerya et al., 2002). The amphibolite-facies mélange zone may have also developed over a much shorter period of time than others that record larger temperature disparities.

Few studies have quantified the timescale of tectonic mélange formation, especially in relation to the recorded spatial scale of mixing. Elucidating this timescale is particularly important for interpreting the tectonic and geochemical evolution of mélange zones, especially rates of mass transport (e.g., Bebout & Barton, 1993; Penniston-Dorland et al., 2012, 2014; Sorensen & Grossman, 1989), tectonic mixing (e.g., Bebout & Barton, 2002; King et al., 2006, 2007; Penniston-Dorland et al., 2018) and for understanding timescales of localized penetrative deformation within mélange relative to large-scale processes such as underplating (e.g., Agard et al., 2018). Here, we use Sm-Nd garnet geochronology to assess temporal variations in the timing of peak metamorphism of mélange blocks throughout the amphibolite-facies mélange zone of the Catalina Schist. We compare these data to prior geochronologic data results to understand the relationship between spatial and temporal scales of mixing within the mélange zone. We then interpret structural relationships between the mélange zone and other tectonometamorphic units of the Catalina Schist, and specifically address the temporal relationship between the formation of the mélange zone and metamorphism of an underlying coherent amphibolite unit. Importantly, this work illuminates how feedbacks between matrix rheology and the timescale over which a mélange zone develops affect the degree of tectonic mixing.

2. Geologic Background

The Catalina Schist, best exposed on Santa Catalina Island (California, USA), consists of several tectono-metamorphic units separated by subhorizontal thrusts. These thrust sheets form an inverted metamorphic sequence ranging in grade from lawsonite albite to upper amphibolite facies (see Figures 1a and 1b; Grove & Bebout, 1995; Platt, 1975, 1976). Each thrust sheet consists of both structurally coherent metamafic and metasedimentary units as well as mélange. The mélange zones appear to be intercalated with the coherent units, which are structurally continuous at the sub-km to km-scale (Bebout & Barton, 1993). Within the mélange zones, sub-cm to 100-m sized metasedimentary, mafic and ultramafic blocks are encapsulated within a deformed, fine-grained heterogeneous matrix. This matrix is a chemical and isotopic mixture of the mafic, ultramafic and metasedimentary materials that comprise the mélange zone (Bebout & Barton, 1989, 1993, 2002; Sorensen, 1984; Sorensen & Barton, 1987). Pressure-temperature estimates for the units are summarized in Figure 1c, and include multi-phase thermobarometry (e.g., Platt, 1975; Sorensen & Barton, 1987), generalized phase equilibria modeling (Grove & Bebout, 1995), Zr-in-rutile thermometry (K. M. Harvey et al., 2021; Penniston-Dorland et al., 2018), and quartz-in-garnet elastic thermobarometry (K. M. Harvey et al., 2021), and are summarized in Figure 1c. Previous constraints using Lu-Hf garnet and U-Pb titanite geochronology imply amphibolite-facies metamorphism occurred between ca. 115 and 110 Ma (Anczkiewicz et al., 2004; Mattinson, 1986). Metamorphism of the lower grade units is younger, and ranges in age from ca. 109 to 97 Ma based on K-Ar and $^{39}Ar/^{40}Ar$ white mica and hornblende ages that are interpreted to represent peak or near-peak metamorphism as well as U-Pb detrital zircon (Grove & Bebout, 1995; Grove et al., 2008; Suppe & Armstrong, 1972).

The amphibolite-facies mélange zone is primarily composed of garnet amphibolite and serpentinite blocks, with rare metasedimentary rocks including metachert and metagraywacke, encapsulated within a heterogeneous matrix. The matrix can broadly be subdivided into two distinct mafic-ultramafic compositions with different deformation features (see Bebout & Barton, 2002). The first matrix is a siliceous and composed of radiating anthophyllite or enstatite plus talc and often chlorite. This matrix is most commonly associated with massive serpentinite blocks and generally shows little evidence of deformation. The second matrix composition is aluminous and composed primarily of folded or crenulated sheet silicates including chlorite, biotite and talc as well as clinoamphiboles such as hornblende or actinolite. This matrix is most often associated with the mafic blocks and is generally more deformed than the siliceous matrix. The two matrix compositions appear to be intercalated at the sub-km scale (Bebout & Barton, 2002).

Blocks throughout the zone record temperatures between 640 and 740°C (K. M. Harvey et al., 2021; Penniston-Dorland et al., 2018) and pressures of 1.3–1.4 GPa (K. M. Harvey et al., 2021). These conditions require thermal gradients that are much higher than average conditions recorded by other exhumed subduction terranes (see compilation by Penniston-Dorland et al. [2015]). Mechanisms to explain these anomalously high temperature conditions include high thermal gradients during nascent subduction and formation of the amphibolite units within a forearc thrust system (e.g., Grove et al., 2008; Platt, 1975). However, subduction initiated in the region at ca. 140 Ma (Grove et al., 2008; Morton et al., 2014; Shaw et al., 2003; Suppe & Armstrong, 1972), and petrologic evidence suggests that the unit still formed at the subduction interface (K. M. Harvey et al., 2021; Penniston-Dorland et al., 2018).

Multiple lines of evidence suggest that the amphibolite-facies mélange zone formed by progressive tectonic and metasomatic mixing along a small region of the subduction interface rather than by sedimentary processes. First, the unique hybrid matrix compositions observed throughout mélange zone are difficult to explain by a sedimentary mechanism (Bebout & Barton, 2002; King et al., 2006). Second, geochemical and petrologic evidence from metasomatic reaction rinds found at the contact between blocks and matrix suggest that the matrix formed by progressive alteration and ablation of the blocks throughout prograde and peak metamorphism (i.e., Penniston-Dorland et al., 2014). Third, the matrix records similar peak metamorphic conditions to the blocks (see Penniston-Dorland et al., 2018), making a sedimentary origin unnecessary. Within the context of these observations, the small yet resolvable temperature variations observed among the mélange blocks have previously been interpreted to reflect tectonic mixing by mélange flow zone along a ~20 km region of the subduction interface, corresponding to a difference in burial depth of ~7 km (assuming an average thermal gradient of 15°C/km and a slab dip of 20°; Penniston-Dorland et al., 2018 updated by K. M. Harvey et al. [2021]). This is expected to produce lithostatic pressure variations of <0.2 GPa,

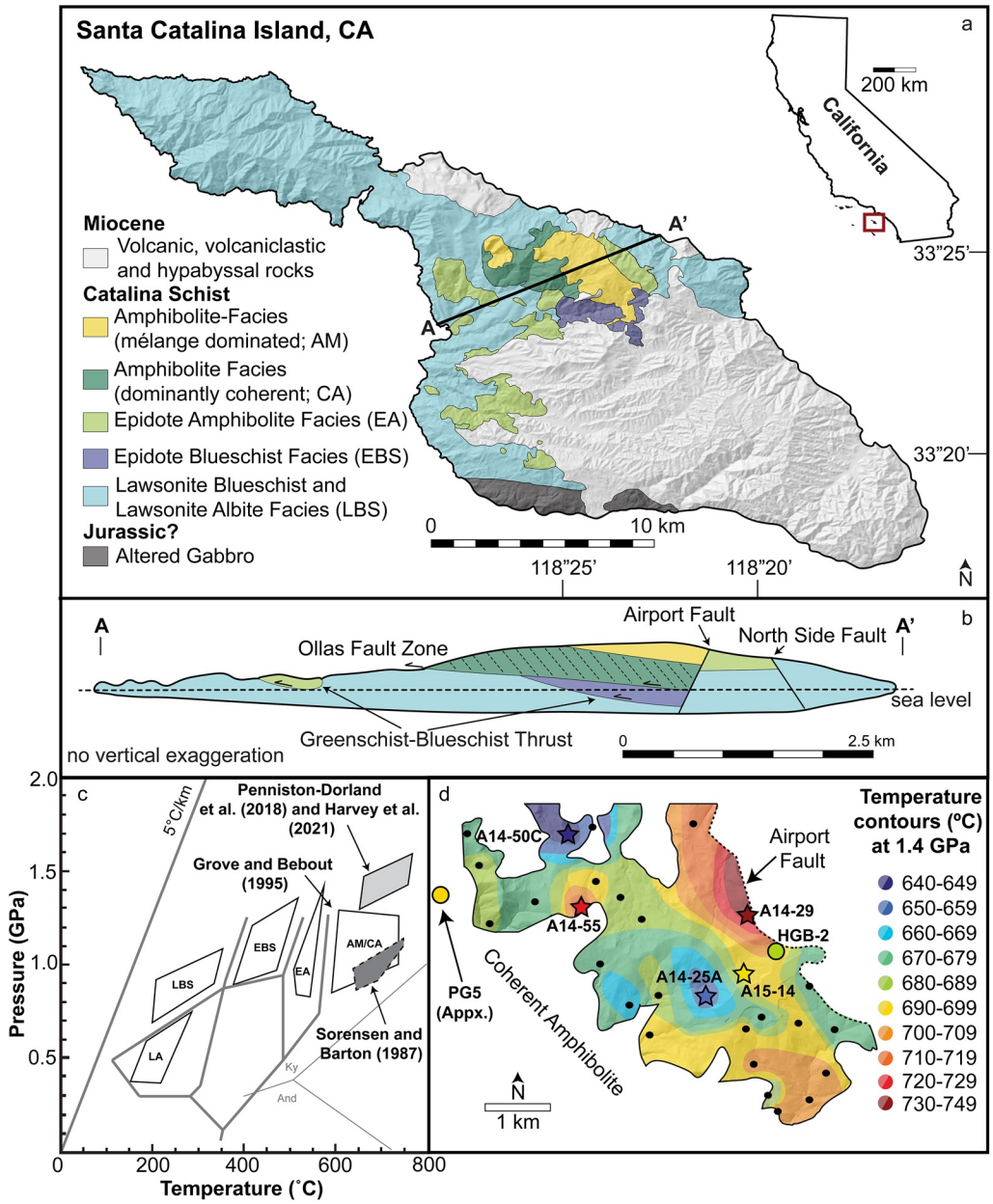

Figure 1. (a) Geologic map and (b) cross-section of the Catalina Schist based on Platt (1975, 1976) showing the structural relationship between the tectonometamorphic units. In the cross-section, inclined lines in the coherent amphibolite unit indicate general foliation orientation. Basemap source: USGS (2021). (c) Pressure-temperature estimates for the tectonometamorphic units of the Catalina Schist modified after Grove and Bebout (1995). Estimates shown for the amphibolite-facies units are based on generalized phase equilibria modeling (Grove & Bebout, 1995), multi-phase thermobarometry and fluid inclusions (Sorensen & Barton, 1987), and Zr-in-rutile thermometry and quartz-in-garnet elastic barometry (K. M. Harvey et al., 2021; Penniston-Dorland et al., 2018). (d) Contour map showing the distribution of peak metamorphic temperatures recorded by blocks and matrix throughout the amphibolite-facies mélange zone determined by Zr-in-rutile thermometry and estimated at 1.4 GPa (modified from Penniston-Dorland et al. [2018] with updated temperature estimates from K. M. Harvey et al. [2021]). The locations of samples considered in this study are shown as stars. Two additional samples, HGB-2 (mélange block; Sorensen, 1988; Zack et al., 2004) and PG5 (coherent amphibolite; Anczkiewicz et al., 2004; location is approximate), are shown as a circles. All symbols are colored based on the peak Zr-in-rutile temperature recorded by the block (see text).

consistent with the observed peak pressures recorded by quartz-in-garnet barometry (1.3–1.4 GPa; K. M. Harvey et al., 2021).

3. Methods

3.1. Garnet Major and Trace Element Compositions

Garnet major element compositions were determined by wavelength dispersive spectroscopy (WDS) using the JEOL JXA 8900R Electron Probe Microanalyzer (EPMA) housed in the AIMLab at the University of Maryland. Measurements were made using a 15 kV accelerating voltage, a beam current of 25 nA, and a beam diameter of 1 μm. Analyses were standardized using natural mineral standards and processed using a ZAF correction scheme (Armstrong, 1988). Select garnets in each sample were additionally chosen for WDS X-ray maps to fully assess major element zoning. X-ray maps were collected using a 15 kV accelerating voltage, a beam current of 250 nA and a beam diameter between 5 and 20 μm.

Trace element zoning was determined by laser ablation inductively coupled plasma mass spectrometry (LA-ICP-MS) using the Thermo-Fisher Element 2 magnetic sector mass spectrometer coupled to a Nu-Wave UP213 solid state Nd:YAG laser ablation system housed in the Plasma Laboratory at the University of Maryland. Analyses were collected using 55 μm spots, a repetition rate of 7 Hz, and a fluence of 3–5 J/cm^2. Data were processed using Iolite v4 (Paton et al., 2011). Raw counts were standardized against the glass standard NIST612 (Jochum et al., 2011) and normalized to ^{29}Si. BHVO-2G glass (Jochum et al., 2005) was used as a secondary standard to assess data reproducibility. Isotopes analyzed include ^{29}Si, ^{90}Zr, ^{137}Ba, ^{139}La, ^{140}Ce, ^{141}Pr, ^{146}Nd, ^{147}Sm, ^{153}Eu, ^{155}Gd, ^{157}Gd, ^{159}Tb, ^{163}Dy, ^{165}Ho, ^{167}Er, ^{169}Tm, ^{173}Yb, ^{175}Lu, and ^{179}Hf.

3.2. Sm-Nd Garnet Geochronology

Garnet separates were prepared from a representative fraction of each sample by hand crushing using steel and agate mortar and pestles, magnetic separation and hand picking. Each separate was then hand crushed using an agate mortar and pestle to between 75 and 150 μm for chemical preparation. Powder fractions (grain sizes <75 μm) were also collected for analysis and are indicated in the results by "Pwd." Partial dissolution (Baxter et al., 2002; Dragovic et al., 2012; Pollington & Baxter, 2011; Starr et al., 2020) was used to remove any recalcitrant micro-inclusions such as apatite, epidote and hornblende that may significantly affect on the isotopic data. Aliquots between 40 and 130 mg of the garnet and garnet powder separates were first chemically leached in 2 mL of 7 N nitric acid (HNO_3) for 2 h at 120°C to remove easily dissolved non-silicate phases. The garnet separates were then added to low concentration hydrofluoric acid (HF) (~1–8%) for two hours at 120°C, with the concentration of HF set according to the desired amount of dissolution. Another HNO_3 stage of dissolution removed any secondary fluorides produced during the preceding HF dissolution. The HF and HNO_3 stages were repeated with varying concentrations of HF until the samples reached a mass loss between 70% and 90%. Leachates produced during each dissolution stage were collected for analysis and are indicated in the results by "Lch." Following partial dissolution, each sample was fully dissolved using a combination of concentrated HNO_3, HF and hydrochloric acid (HCl).

Whole rock separates were also prepared for analysis. A representative fraction (30–50 g) of each sample was hand crushed and then powdered using a ceramic ball mill. Between 30 and 100 mg of each whole rock powder was then fully dissolved using a combination of HNO_3, HF, and HCl.

After full dissolution, all samples were spiked with an in-house mixed ^{147}Sm-^{150}Nd spike prior to chemical separation by column chromatography (J. Harvey & Baxter, 2009). Samples were first loaded in a cation exchange column using AG50w-X4 resin with HCl to remove Fe and other 2+ cations that interfere with subsequent column separation steps. The rare earth elements (REE) were then isolated using Eichrom TRU spec resin with HNO_3. Finally, Sm and Nd were separated using AG50w-X4 resin with in-house distilled 2-methyl lactic acid (MLA). Full-procedure and 3-column blanks were run alongside the samples. Blank concentrations for the lab were all <5 pg Nd.

Samples were analyzed at the Boston College Center for Isotope Geochemistry using an IsotopX Phoenix Thermal Ionization Mass Spectrometer (TIMS). For each sample, 1.7–16.3 ng of NdO was loaded onto outgassed rhenium filaments in Ta_2O_5 activator slurry, and 1.7–46 ng of Sm was loaded in HNO_3 onto

Table 1
Data Summary

Sample	Zr-in-rutile temperature (°C)	Sm-Nd garnet age (Ma)	Garnet grain size (mm)	Assemblage	Garnet inclusion assemblage
A14-50C	643 ± 6	111.1 ± 2.9	≤0.3	Grt + Hbl + Qtz + Rt + Ttn + Ap + Zrc	Hbl + Ttn + Rt + Qtz + Ap + Zrc
A14-25A	655 ± 7	111.5 ± 0.9	≤8.0	Grt + Hbl + Saussurite + Zo + Ep + Rt + Ttn + Zrc	Hbl + Rt + Pl + Ep + Ap + Zrc
A15-14	695 ± 13	109.9 ± 1.2	≤1.5	Hbl + Grt + Rt + Ap + Zrc	Hbl + Rt + Ap + Zrc
A14-55	721 ± 11	115.5 ± 3.0	≤3.0	Grt + Hbl + Pl + Chl + Qtz + Rt + Zrc	Hbl + Rt + Pl + Qtz + Zrc
A14-29	735 ± 8	107.7 ± 5.5	≤1.7	Grt + Hbl + Ph + Ep + Rt + Qtz + Chl + Zrc	Hbl + Ep + Rt + Ph + Qtz + Zrc

Note. Zr-in-rutile data from Penniston-Dorland et al. (2018) recalculated at 1.4 GPa after K. M. Harvey et al. (2021). Data are from matrix rutile (see Penniston-Dorland et al., 2018). Sm-Nd garnet ages are the preferred age for each sample (see text for additional details). Mineral abbreviations (after Whitney & Evans, 2010): Ap, apatite; Chl, chlorite; Ep, epidote; Hbl, hornblende; Ph, phengite; Pl, plagioclase; Qtz, quartz; Rt, rutile; Ttn, titanite; Zrc, zircon; Zo, zoisite.

tantalum center filaments. In-house standard solutions of Sm and Nd (AMES metal) were used to assess long-term reproducibility over the period of analysis. For Nd, 4 ng loads of the standard solution yielded $^{143}Nd/^{144}Nd = 0.512152 \pm 9$ (17.6 ppm, 2sd; $n = 36$). For Sm, 20 ng loads of the standard solution yielded $^{147}Sm/^{152}Sm$ of 0.560855 ± 44 (78.2ppm, 2sd; $n = 21$). Repeat analyses of mixed gravimetric normal solutions with a calibrated in-house spike yield a reproducibility of 0.054% for $^{147}Sm/^{144}Nd$.

4. Results

Five metamafic garnet amphibolite blocks from the amphibolite-facies mélange zone were analyzed. The peak metamorphic temperature for each sample was determined by Zr-in-rutile thermometry by Penniston-Dorland et al. (2018) and updated using the most recent combined experimental-empirical thermometer calibration (Kohn, 2020) by K. M. Harvey et al. (2021). Figure 1d shows peak temperatures estimated at 1.4 GPa based on quartz-in-garnet barometry (K. M. Harvey et al., 2021) for the samples relative to other blocks in the mélange zone (see Penniston-Dorland et al., 2018 for methods and sample locations). These five blocks record temperatures between 643 and 735°C, spanning the range of peak metamorphic temperatures observed throughout the mélange zone.

4.1. Sample Descriptions

Samples contain garnet + hornblende ± epidote ± plagioclase ± quartz + rutile ± titanite ± apatite + zircon. The peak metamorphic temperature determined by Zr-in-rutile on matrix rutile (from Penniston-Dorland et al., 2018), Sm-Nd garnet age, mineral assemblage and garnet inclusion assemblage for each sample are summarized in Table 1. Detailed descriptions, including additional major and trace element data, are provided on a sample-by-sample basis in the Supporting Information S1, and only a brief summary of general trends is provided here, especially emphasizing major and trace element zoning (Figure 2). Garnet porphyroblasts range in size from ~0.3 to 8 mm in diameter. Most are concentrically zoned and preserve prograde growth zoning including Mn and heavy REE-enrichment in garnet cores and middle REE-enrichment in garnet rims (e.g., Cheng et al., 2008, 2010, 2018; Hickmott & Spear, 1992; Hickmott et al., 1987; Hollister, 1966; Kohn, 2009; Lapen et al., 2003; Skora et al., 2006; Smit et al., 2013). Sample A14-29 shows prograde REE zoning but no variation in Mn. Similarly, sample A15-14 shows no major element zoning and enrichment of Sm toward the geometric center of garnet rather than the rim. None of the blocks show evidence for significant retrogression or overprinting at sub-amphibolite-facies conditions, although one does display minor resorption and replacement of garnet by chlorite (A14-55) and in another rutile is partially replaced by titanite (A14-25A). Sm/Nd inferred from LA-ICP-MS ranges from 0.3 to 5.8.

4.2. Sm-Nd Garnet Geochronology

For all samples except A14-29, Sm and Nd concentrations in garnet determined by TIMS and LA-ICP-MS show good agreement (Supporting Information S1). Overall, Sm concentrations determined by TIMS versus LA-ICP-MS are 0.43–5.50 ppm and 0.06–5.30 ppm respectively, while Nd concentrations are 0.17–1.95

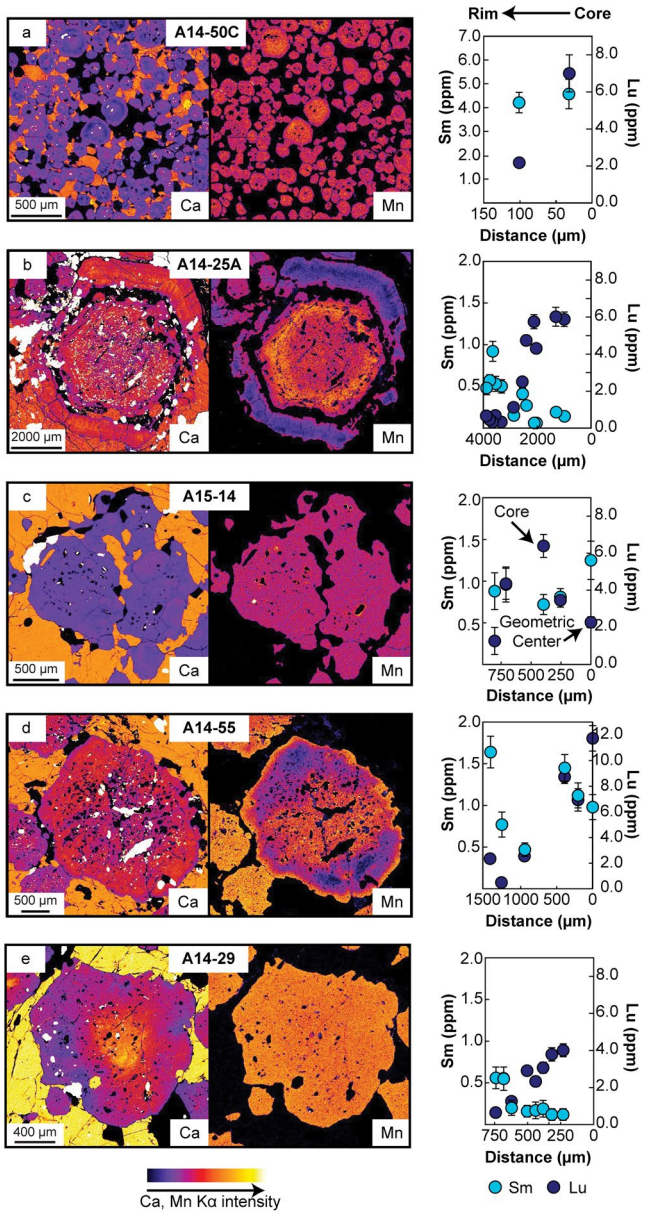

Figure 2. X-ray maps and trace element traverses of garnet porphyroblasts for samples (a) A14-50C, (b) A14-25A, (c) A15-14, (d) A14-55, and (e) A14-29 showing zoning in Ca, Mn, Lu, and Sm for each sample. Trace element traverses are shown from core (right; 0 µm) to rim (left).

ppm; (TIMS) and b.d.–2.15 ppm (LA-ICP-MS). Concentrations of Nd determined by LA-ICP-MS for A14-29 are all less than 0.2 ppm while concentrations determined by TIMS range between 0.49 and 0.64 ppm. Given the moderate $^{147}Sm/^{144}Nd$ determined for the sample (0.76–0.99 for garnet residues), these differences may reflect incomplete cleansing of garnet separates (i.e., TIMS concentrations are higher). Compositional layering within the sample suggests bulk rock heterogeneity.

Whole rock concentrations determined by TIMS range from 1 to 66 ppm Sm and 5–364 ppm Nd. Two whole rock separates (A14-55 and A14-50C) record unusually high Sm and Nd concentrations. These concentrations were externally verified by ICP-MS to rule out contamination (see Supporting Information S1) and are consistent with REE enrichment via metasomatism, which was previously reported for the terrane (Sorensen & Grossman, 1989).

Isotopic data determined by TIMS are reported in Table 2. The reported uncertainties reflect either the internal precision of the analysis or the external precision based on the long-term reproducibility of the in-house AMES metal standards, whichever is higher. Garnet, garnet powder and garnet leachate $^{147}Sm/^{144}Nd$ range from 0.45 to 2.1, but the majority of the separates record $^{147}Sm/^{144}Nd \geq 1$, suggesting that garnet separates were sufficiently cleansed of inclusions to determine an accurate garnet age (Baxter et al., 2017). Whole rocks record $^{147}Sm/^{144}Nd$ between 0.11 and 0.21. Sm-Nd isochrons were constructed using IsoplotR (Vermeesch, 2018). The preferred age for each sample is shown in bold in Figure 3 and reported in Table 1. Uncertainties are reported as either as 2σ or as 2σ times the square root of the MSWD for samples with elevated MSWDs (4.4–7.6; chi-square p-value < 0.05). Multiplying the uncertainty by the square root of the MSWD assumes that all analytical uncertainties have been underestimated by this factor. While this is likely not a valid assumption (see Section 5.1), the inflated uncertainties are viewed as reasonable estimates of the uncertainty in the isochron-derived age. The preferred age and uncertainty for each sample is shown in bold in Figure 3 and reported in Table 1. Separates that fall well outside the uncertainty of the isochron were excluded to determine the preferred ages for samples A14-25A (Grt1), A15-14 (Grt2, Grt4) and A14-55 (Grt2). All of the excluded separates record similar Sm and Nd concentrations to other separates from the same sample; however, they do not appear to be from the same age population. Two-point isochrons between these separates and the whole rock are reported in Figure 3 and are all either resolvably older (A14-25A Grt1, A15-14 Grt2) or younger (A15-14 Grt4, A14-55 Grt2) than the primary garnet population. The preferred bulk garnet ages for the five samples range from 115.5 ± 3.0 to 107.7 ± 5.5 Ma (Table 1), with uncertainties between 0.9 and 5.7 Ma. Although most of the ages overlap within uncertainty, age variations are resolvable. Potential explanations for the significant scatter in the data and resulting elevated age uncertainties are discussed in Section 5.1.

5. Discussion

5.1. Interpreting Bulk Garnet Ages

While the samples have elevated MSWDs (up to 7.6 for preferred ages), reflecting scatter in the isotopic data about the best-fit line, it is unlikely that this reflects contamination by REE-bearing inclusions (e.g., Baxter & Scherer, 2013; Scherer et al., 2000; Thöni, 2002). The high $^{147}Sm/^{144}Nd$ (>1) recorded by garnet, garnet powder and garnet leachate separates, and the generally good agreement between LA-ICP- MS and TIMS

Table 2
Sm-Nd Isotopic Data for Garnet and Whole Rock Separates

	% Mass loss	Nd (ppm)	Sm (ppm)	$^{147}Sm/^{144}Nd$	±2 S.E.	$^{143}Nd/^{144}Nd$	±2 S.E.	$^{143}Nd/^{144}N$ (ppm, 2 S.E.)
A14-50C								
Grt1	91	1.866	5.526	1.79115	0.00097	0.513596	0.000009	17.6
Grt2	76	1.946	5.497	1.70879	0.00092	0.513548	0.000011	21.4
Grt Pwd	69	1.638	3.688	1.36218	0.00074	0.513270	0.000009	17.6
WR	–	363.921	66.021	0.10974	0.00006	0.512378	0.000009	17.6
A14-25A								
Grt1	73	0.243	0.626	1.55808	0.00084	0.513931	0.000011	21.2
Grt2	83	0.194	0.620	1.93807	0.00105	0.514180	0.000009	17.6
Grt3	81	0.197	0.625	1.91618	0.00103	0.514166	0.000015	29.2
Grt4	84	0.176	0.591	2.02500	0.00109	0.514227	0.000021	40.8
Grt Pwd	90	0.172	0.583	2.05405	0.00111	0.514263	0.000012	22.5
Grt2 Lch	–	0.212	0.557	1.58819	0.00086	0.513939	0.000026	50.6
WR	–	37.248	13.117	0.21301	0.00012	0.512923	0.000009	17.6
A15-14								
Grt1	78	0.484	0.891	1.11380	0.00060	0.51349	0.000014	27.3
Grt2[a]	82	0.511	1.023	1.21129	0.00065	0.51367	0.000017	33.1
Grt3	79	0.307	0.595	1.17452	0.00063	0.51346	0.000011	21.4
Grt4	77	0.455	0.903	1.19914	0.00065	0.51353	0.000011	22.3
Grt Pwd	87	0.194	0.561	1.74763	0.00049	0.51394	0.000009	17.6
Grt2 Lch	–	0.429	0.638	0.89964	0.00094	0.51333	0.000009	17.6
WR	–	221.621	36.775	0.10045	0.00005	0.51277	0.000009	17.6
A14-55								
Grt1	82	0.379	0.850	1.35773	0.00073	0.513772	0.000009	17.6
Grt2[a]	79	0.341	0.690	1.22490	0.00066	0.513587	0.000014	27.2
Grt3	78	0.367	0.851	1.40343	0.00076	0.513788	0.000009	17.6
Grt4	81	0.366	0.834	1.37914	0.00074	0.513775	0.000011	21.8
Grt Pwd	84	0.307	0.663	1.30827	0.00071	0.513738	0.000009	17.6
WR	–	46.45	13.549	0.17642	0.00010	0.512874	0.000009	17.6
A14-29								
Grt1	80	0.490	0.801	0.98985	0.00053	0.513503	0.000009	17.6
Grt2	78	0.645	0.814	0.76368	0.00041	0.513318	0.000009	17.6
Grt1 Lch1	–	0.576	0.426	0.44763	0.00024	0.513104	0.000009	17.6
Grt1 Lch2	–	0.590	0.782	0.80125	0.00043	0.513349	0.000010	20.0
WR	–	5.256	1.206	0.13883	0.00007	0.512897	0.000009	17.6

Note. Grt, garnet; Pwd, powder; Lch, leachate; WR, whole rock.
[a]Excluded from isochron (see discussion).

Sm and Nd concentrations both support the view that the separates were sufficiently cleansed. Instead, elevated MSWDs are expected for high-precision isotope measurements and likely reflect real variations in garnet crystallization age, perhaps indicating age zonation within single crystals (Kohn, 2009; Pollington & Baxter, 2011). Similarly, analyses that fall significantly above or below the isochron likely indicate the presence of either older (A15-14; see Figure 3) or younger (A14-55) garnet populations, although without

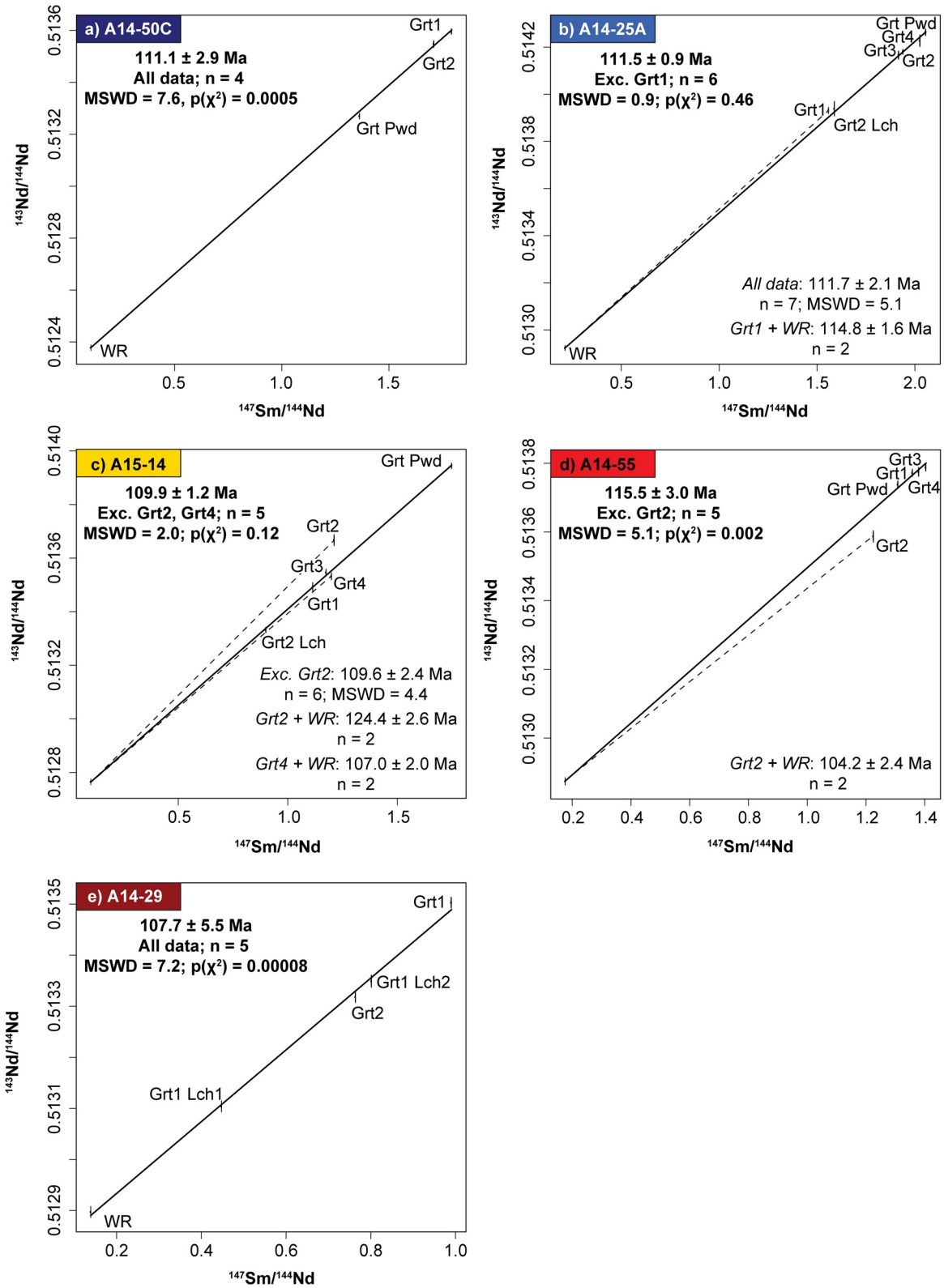

Figure 3. Garnet-whole-rock Sm-Nd isochrons for samples (a) A14-50C, (b) A14-25A, (c) A15-14, (d) A14-55, and (e) A14-29. The final reported age uncertainty is reported either as 2σ confidence or as 2σ times the square root of the MSWD for samples with elevated MSWDs (4.4–7.6; chi-square p-value < 0.05). The preferred age for each sample is shown in bold with excluded analyses indicated as "Exc." (see text for additional details).

additional chronologic constraints (e.g., from zoned garnet geochronology) it is not possible to assess the span of ages recorded by each sample.

The interpretation of ages determined from bulk garnet separates depends largely on the initial distribution of the parent isotope and the volumetric abundance of each growth zone. For example, even though garnet cores are not volumetrically significant and will therefore represent a small fraction of the bulk separate, Lu is strongly enriched in garnet cores relative to the rims (e.g., Bloch et al., 2015; Hickmott & Spear, 1992; Hickmott et al., 1987; Kohn, 2009; Skora et al., 2006). Because of this, bulk Lu-Hf ages are generally interpreted to reflect earlier prograde garnet growth (e.g., Cheng et al., 2010; Lapen et al., 2003). In contrast, light and middle rare earth elements are generally enriched in garnet rims relative to garnet cores. Because of this enrichment and because the garnet rim is volumetrically more abundant than the core, bulk garnet Sm-Nd ages are often interpreted to reflect growth of garnet approaching peak metamorphic conditions (Baxter & Scherer, 2013; Kohn, 2009; Lapen et al., 2003).

Two primary observations support the interpretation that garnet in the five samples considered in this study crystallized during prograde and peak metamorphism and that the bulk Sm-Nd ages likely represent garnet growth spanning near- to peak-metamorphism. First, the peak assemblage (hornblende + rutile ± plagioclase) is found as inclusions within garnet in all samples. The absence of an earlier inclusion assemblage suggests garnet grew during amphibolite-facies metamorphism. Second, garnet displays typical prograde major and trace element zoning in most of the samples, with the exception of A15-14 (Figures 2 and 3). The heavy REEs, including Lu, are enriched toward the garnet cores in all samples while the light/middle REEs are generally enriched toward the garnet mantles/rims. If garnet volume increased uniformly with temperature (e.g., through continuous chlorite breakdown) or if garnet nucleation was significantly overstepped, the reported Sm-Nd ages likely approach the timing of peak metamorphism of each sample. Samples A14-50C and A15-14 show no obvious enrichment in Sm toward the garnet rims, so the reported ages might reflect growth at somewhat lower P-T conditions.

5.2. Impact of REE Diffusion

Diffusion of Nd in garnet at high temperatures can potentially reset (fully or partially) the Sm-Nd isotopic system, resulting in recorded ages that are significantly younger than the true timing of peak metamorphism. Although diffusion of REEs in garnet is slow relative to major elements such as Mn (e.g., Carlson, 2006; Chakraborty & Ganguly, 1992; Tirone et al., 2005), some diffusional modification is possible at the peak metamorphic conditions reached by these samples (e.g., Baxter & Scherer, 2013; Bloch & Ganguly, 2015; Bloch et al., 2020; Carlson, 2006, 2012; Kohn, 2009; Smit et al., 2013). The degree of diffusional resetting is primarily dependent on three factors: the size of the garnet grains, the maximum temperature, and the duration of metamorphism at maximum temperatures. Small grains (0–1 mm) like those observed in sample A14-50C can be partially reset at 700°C in as little as 10 kyr and fully reset in 1–10 Myr (Baxter & Scherer, 2013). In contrast, larger grains (~5 mm) like those observed in A14-25A require durations of metamorphism on the order of 100 Myr at 700°C to completely reset the Sm-Nd system.

While it is likely that these samples experienced some diffusional modification, the degree of modification is difficult to quantify. In the case of significant diffusional modification, it is expected that the smallest garnet grains would experience the highest degree of resetting and thus record the youngest ages. There is no obvious correlation between garnet grain size and the age recorded by each sample (see Figure 2, Table 1), suggesting limited diffusional resetting. Additionally, retention of Mn zoning in samples A14-25A, A14-50C and A14-55 favors the interpretation that the duration of amphibolite-facies metamorphism was relatively short (e.g., Carlson, 2006; Chakraborty & Ganguly, 1992). In that case, significant modification of Sm-Nd systematics is not expected. Samples A14-29 and A15-14, on the other hand, do not preserve any significant zoning in Mn. This may indicate that these two samples experienced more diffusional modification of the Sm-Nd system, although A14-29 still records prograde REE zoning. It is possible that the single garnet separate that falls above the isochron for sample A15-14 reflects growth of garnet during an early metamorphic event at or before ca. 124 Ma that was largely reset to give a bulk garnet age of ca. 109 Ma (Figure 3).

Two primary lines of evidence suggest that the long timescales of high-T metamorphism that would be required for significant diffusional resetting are unlikely: (a) the preservation of Mn zoning in all but two

samples and the preservation of prograde REE zoning in all but one sample and (b) the lack of correlation between age and garnet grain size both suggest garnets are not significantly reset. On this basis, the Sm-Nd ages are interpreted to represent the timing of peak metamorphism.

5.3. Age and Temperature Variations Within the Amphibolite-Facies Mélange Zone

The amphibolite-facies mélange zone was previously interpreted to have formed by chaotic tectonic mixing via mélange flow throughout prograde and peak metamorphism (Penniston-Dorland et al., 2018). In this model, metamorphism and mélange formation are genetically related such that blocks sourced from various depths are juxtaposed through a combination of forced updip transport driven by narrowing of the subduction interface at depth and shearing between mélange components with contrasting rheologic behavior. Mafic, metasedimentary and ultramafic blocks within the mélange zone are sourced from both the down-going slab and overriding plate by fluid-mediated mechanical disaggregation. The surrounding matrix is derived by progressive metasomatism and ablation of the blocks, resulting in a unique hybrid composition (Bebout & Barton, 2002; King et al., 2006, 2007; Penniston-Dorland et al., 2014). Geochemical and isotopic evidence for tectonic mélange formation occurs both within the low-grade lawsonite albite (~0.4–0.7 GPa; Grove & Bebout, 1995) and lawsonite blueschist-facies (~0.7–1.1 GPa; Grove & Bebout, 1995) mélange zones as well as the high-grade amphibolite-facies mélange zone (e.g., Bebout & Barton, 2002; King et al., 2006; Penniston-Dorland et al., 2014; Sorensen & Grossman, 1989) indicating that mélange formation likely began at relatively shallow depths (≤15 km) and tectonic mixing progressed throughout prograde and peak metamorphism.

Formation of mélange via prograde mechanical mixing is further supported by enrichment of Mg in the core of reaction rind garnet compared to mafic block garnet within the amphibolite-facies mélange zone. Mg-enrichment is attributed to mélange-forming mechanical mixing processes (Bebout & Barton, 2002; Penniston-Dorland et al., 2014). The difference in compositions between garnet in the block interior and in the reaction rind, paired with thermodynamic modeling that indicates that both nucleated at amphibolite-facies conditions, requires that metasomatism of the block related to mélange formation must have occurred prior to garnet growth (Penniston-Dorland et al., 2014).

Within the context of extensive field and geochemical evidence for tectonic mixing, the non-systematic distribution of peak metamorphic temperatures among blocks recorded by Zr-in-rutile thermometry as well as larger pressure-temperature disparities recorded by Zr-in-rutile thermometry and quartz-in-garnet barometry among blocks within epidote amphibolite-facies mélange zones further support the mélange flow model (K. M. Harvey et al., 2021; Penniston-Dorland et al., 2018). This model predicts a random distribution of ages and temperatures. Other potential explanations for age and temperature variations within the mélange zone are discussed below.

Conceivably, systematic temperature variations within the mélange zone could be obscured by complex structures including large-scale synforms and antiforms, or metamorphism could be decoupled temporally from the formation of the mélange. If so, temperature variations among blocks may be systematic and result from temporal variations in thermal structure. Diverse tectonic processes could drive progressive heating or cooling of the interface and lead to systematic age-temperature distributions among blocks. For example, rapid cooling is expected following subduction initiation as the mantle wedge becomes hydrated and the system approaches steady-state conditions (e.g., Gerya et al., 2002; Ishizuka et al., 2011; Peacock, 1991, 1996; Plunder et al., 2015; Wakabayashi & Dilek, 2003). Cooling may also be expected following a temperature perturbation (e.g., as the result of cooling following slab rollback, etc.) as the system returns to steady-state conditions. In these cases, hotter blocks might be expected to have older ages. Alternatively, progressive heating might occur during upwelling of hot mantle via either slab rollback or a slab hole/window (e.g., Abratis & Wörner, 2001; Menant et al., 2016; Thorkelson et al., 2011) or during subduction of a seamount or ridge (e.g., DeLong et al., 1979; Iwamori, 2000; Santosh & Kusky, 2010; Spinelli & Harris, 2011). In these cases, hotter blocks might be expected to have younger ages.

Garnet amphibolite blocks from the mélange zone record Sm-Nd garnet ages between ca. 108 and 116 Ma. Age variations among the blocks are small but resolvable. An additional block, "HGB-2" (Sorensen, 1988), records a minimum age of metamorphism of 111.7 ± 1.5 Ma via a U-Pb isochron age of overprinting

titanite + garnet + hornblende (Mattinson, 1986). Rutile Zr contents for HGB-2 indicate peak temperatures of 680–700 °C (Z5-129-2a from Zack et al. [2004]; calibration of Kohn [2020], at 1.4 GPa). For these six mélange blocks, age, location within the mélange zone (Figure 4a), and Zr-in-rutile peak metamorphic temperatures (Figure 4b) all appear uncorrelated. While four blocks (A14-50C, A14-25A, A15-14, and A14-29) suggest a trend of decreasing age with increasing temperature, A14-55 records one of the highest temperatures, but the oldest age. Block HGB-2 yields an intermediate temperature and relatively old age. These results suggest that the mélange zone formed over a minimum 7.8 ± 6.3 Myr with a weighted mean age of 111.2 ± 1.1 Ma (MSWD = 3.1; $n = 6$). Because mélange formation likely occurred throughout both prograde and peak metamorphism, this is interpreted as a minimum duration. The lack of correlation (positive or negative) between age and peak metamorphic temperature supports the interpretation that mélange flow was the primary mechanism by which blocks with different peak metamorphic temperatures were juxtaposed. The age difference is significantly shorter than those observed in tectonic mélanges in some other exhumed terranes, which record peak metamorphic age disparities between blocks within individual mélange zones on the order of 30–40 million years (e.g., Krebs et al., 2008; Mulcahy et al., 2018). These differences in duration suggest that the amphibolite-facies mélange zone at Catalina either developed rapidly prior to exhumation or that mixing ceased following development of rheologically strong matrix phases including amphiboles and pyroxenes.

5.4. Comparison With Previous Chronologic Constraints

Three previous studies have placed constraints on the prograde and peak metamorphic history of the amphibolite-facies units. A compilation of all existing chronologic data for these units is shown in Figure 4c. The estimates include U-Pb ages from detrital and metamorphic zircon (Grove et al., 2008) and titanite (Mattinson, 1986) from mélange blocks as well as a Lu-Hf garnet age from the underlying coherent amphibolite unit (Anczkiewicz et al., 2004). Detrital zircon grains from metagraywacke blocks within the mélange zone record a large range of U-Pb ages from Proterozoic to Early Cretaceous (Grove et al., 2008). A weighted mean age of the youngest detrital zircon grains provides a maximum depositional age for the protolith of the metagraywackes of 122 ± 3 Ma. Metamorphic zircon grains from the same rocks record U-Pb ages between 107 and 126 Ma (Grove et al., 2008). This may provide an upper constraint on the earliest stages of mélange zone development, although it is difficult to assess whether the metamorphic zircon ages reflect prograde or peak metamorphism (see Kohn et al., 2015). In addition to the U-Pb age of 111.7 ± 1.5 Ma recorded by sample HGB-2 discussed in Section 5.3, a second garnet amphibolite (91480SC2) records a U-Pb titanite-garnet-hornblende-clinopyroxene isochron age of 114.1 ± 2.1 Ma (Mattinson, 1986). Sample 91480SC2 is float and therefore cannot be linked directly to either the amphibolite-facies mélange zone or the coherent amphibolite; however, the age still reflects amphibolite-facies metamorphism. Finally, a garnet amphibolite from the structurally lower coherent amphibolite unit (PG5) records a Lu-Hf garnet age of 114.5 ± 0.6 Ma (Anczkiewicz et al., 2004). Interestingly, this age exceeds all but one of the amphibolite-facies mélange blocks considered in this study.

Two additional studies have placed constraints on the cooling history of the amphibolite-facies units. K-Ar and $^{40}Ar/^{39}Ar$ ages for hornblende from amphibolite-facies rocks range from 115 to 107 Ma (Grove, 1993; Suppe & Armstrong, 1972). Whether the K-Ar ages are from mélange blocks or underlying coherent amphibolite unit was not specified. The majority of $^{40}Ar/^{39}Ar$ ages come from mafic blocks within the amphibolite-facies mélange zone (Grove, 1993; see summary in Grove and Bebout [1995]). A single $^{40}Ar/^{39}Ar$ hornblende age from the mélange matrix yields an age of ca. 112 Ma. Two ages from the coherent amphibolite yield somewhat younger but overlapping ages between 109 and 107 Ma. The closure temperature for Ar diffusion in hornblende is relatively low (~550°C; Baldwin et al., 1990; Lister & Baldwin, 1996); however, these ages overlap with peak Sm-Nd and U-Pb ages from the unit suggesting limited diffusional resetting. $^{40}Ar/^{39}Ar$ white mica ages from both the mélange zone and coherent amphibolite are younger. White mica from the coherent amphibolite unit records ages between 106 and 101 Ma (Grove & Bebout, 1995). The amphibolite-facies mélange zone records younger white mica ages between 101 and 97 Ma. Given the low closure temperature for Ar diffusion in white mica (~400–450°C; Harrison et al., 2009), these data are interpreted to represent cooling ages for the two units. The implications for potential asynchronous cooling of the two amphibolite-facies units are discussed in Section 5.6.

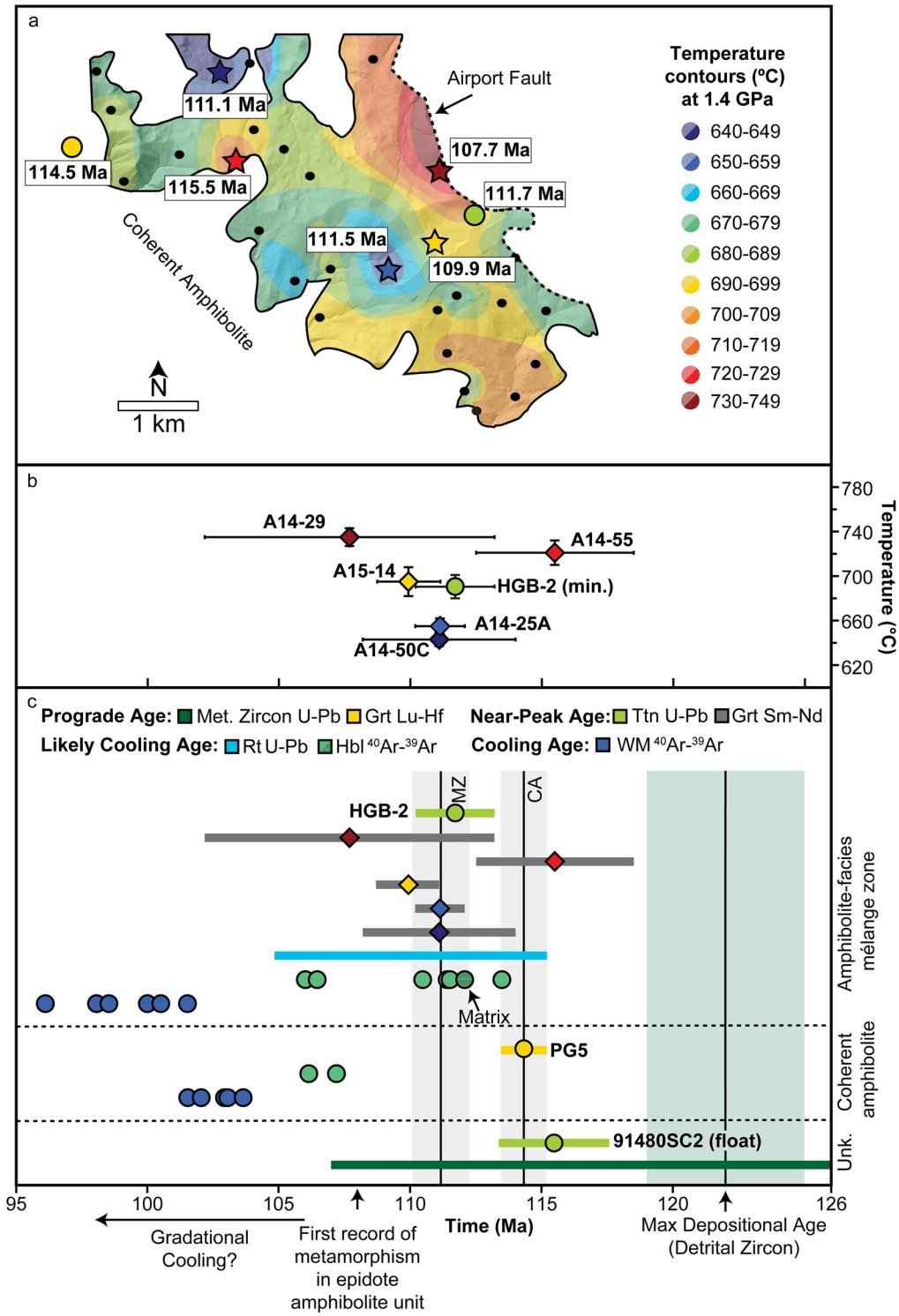

Figure 4.

5.5. Temporal Relationship With the Coherent Amphibolite

The temporal relationship between the amphibolite-facies mélange zone and associated coherent amphibolite unit has important implications for the structural evolution of the terrane. The coherent amphibolite unit occurs beneath the mélange zone, consists of structurally continuous mafic and metasedimentary

rocks and is interpreted to represent an intact slice from the subducting slab (Platt, 1975, 1976; Figures 1a and 1b). Although the two units are structurally and petrologically quite distinct, the coherent amphibolite records similar peak metamorphic temperatures to the mélange zone (690 ± 3°C, estimated by Zr-in-rutile thermometry at 1.4 GPa; K. M. Harvey et al., 2021). The overlap in peak metamorphic temperatures and the current structural position of the two units suggest that the coherent amphibolite represents the subducting slab directly below the amphibolite-facies mélange zone. However, the coherent amphibolite records a Lu-Hf garnet age of ca. 115 Ma (Anczkiewicz et al., 2004) that is on average older than blocks within mélange zone (115–108 Ma; weighted mean of ca. 111 Ma; Figure 4c).

There are multiple possible explanations for the disparity between the Lu-Hf age and the youngest Sm-Nd ages. The first is that the units were metamorphosed simultaneously and the Lu-Hf garnet age represents earlier prograde metamorphism while the Sm-Nd ages approach peak metamorphic conditions. This explanation requires ≥3–7 Myr of garnet growth within the coherent amphibolite unit. Garnet growth durations from similar settings estimated by either zoned chronology or by combining Lu-Hf and Sm-Nd vary between <1 and 25 Myr (e.g., Cheng et al., 2008, 2018; Dragovic et al., 2012, 2015, 2020; Kylander-Clark et al., 2007; Lapen et al., 2003). Although the duration of garnet growth within the coherent amphibolite is currently unconstrained, it is likely that the Lu-Hf age records an earlier stage of garnet growth than the Sm-Nd ages for reasons discussed in Section 5.1.

A second possibility is that garnet in some or all of the samples has been modified by diffusional resetting. As discussed in Section 5.2, diffusional modification of the Sm-Nd system by Nd diffusion would result in ages that are younger than the true peak metamorphic age. Although diffusion of Hf is significantly slower than diffusion of Nd in garnet, any resetting of the Lu-Hf system should result in Lu-Hf ages that are older than the true age of garnet growth (Bloch et al., 2020; Kohn, 2009). A combination of one or both of these diffusion mechanisms would produce a greater apparent disparity between the Lu-Hf and Sm-Nd garnet ages than truly exists (Kohn, 2009). However, for reasons discussed in Section 5.2, diffusional resetting is unlikely to have been significant enough to fully explain this age discrepancy.

The final possibility is that metamorphism of the coherent amphibolite predates the mélange zone and that the contact between the coherent amphibolite and amphibolite-facies mélange zone is post-metamorphic. The scenario requires that the coherent amphibolite was subducted prior to the mélange zone and that the two units were later juxtaposed. This interpretation is supported by field observations that the contact between the coherent amphibolite and mélange matrix and their individual primary foliations are all mutually discordant (Platt, 1976; see Figure 1b). Evidence for shearing at the base of the coherent unit at amphibolite-facies conditions (K. M. Harvey et al., 2021) suggests that the units were juxtaposed near peak metamorphic conditions rather than during later post-metamorphic exhumation. However, juxtaposing an older coherent section of the slab beneath a younger mélange zone raises a number of issues. These include how and where the coherent unit was stored for up to ca. 8 Myr and the mechanism by which the two units were juxtaposed to their current structural positions (i.e., with the older unit below the younger). Additional chronologic and petrologic constraints on the metamorphic history of the coherent amphibolite are needed to fully elucidate the relative importance of these potential explanations.

Figure 4. (a) Contour map of the amphibolite-facies mélange zone showing the distribution of peak metamorphic temperatures and ages (see Figure 1d). (b) Peak metamorphic temperature for each mélange block determined by Zr-in-rutile thermometry (Penniston-Dorland et al., 2018; recalculated by K. M. Harvey et al. [2021]) versus peak metamorphic age determined by Sm-Nd garnet geochronology (colored diamonds) and U-Pb titanite geochronology (gray circle; from Mattinson, 1986). There is no obvious systematic relationship between age and temperature recorded by the blocks. (c) Summary of geochronologic data for the amphibolite-facies units of the Catalina Schist separated by structural position (amphibolite-facies mélange zone, coherent amphibolite, and unknown location). Age estimates from this study are shown as colored diamonds with gray error bars and ordered based on peak metamorphic temperature (Table 1; symbology after panel [a]). Previous age estimates are shown either as filled circles (individual age estimates, uncertainties shown when available) or as ranges represented by colored bars where individual age estimates are not reported. The maximum depositional age of metasedimentary blocks from the amphibolite mélange zone based on detrital U-Pb zircon ages (Grove et al., 2008) is shown as a solid vertical line with uncertainty shown as a light green band. The peak age for the coherent amphibolite (CA) and weighted mean age for the mélange zone (MZ) are shown as solid vertical lines with uncertainty shown as light gray bands. Other data sources: Anczkiewicz et al. (2004), Grove (1993), Grove and Bebout (1995), Grove et al. (2008), Mattinson (1986), and Suppe and Armstrong (1972).

5.6. Timescales of Mélange Development and Underplating

Few studies have specifically quantified the timescale over which tectonic mélange develops; however, this information is critical for interpreting geochemical and structural observations such as evidence for mass transport and deformation. In some terranes, age estimates from blocks within a single mélange zone span tens-of-millions of years. For example, blocks from a single mélange zone can vary in age by as much as 30–40 Myr, for example, the Franciscan Formation in the Tiburon Peninsula (176–145 Ma; Anczkiewicz et al., 2004; Catlos & Sorensen, 2003; Firsov & Dobretsov, 1970; Mulcahy et al., 2018; Suppe & Armstrong, 1972) and Berkeley Hills (163–129 Ma; Anczkiewicz et al., 2004; Mulcahy et al., 2018; Suppe & Armstrong, 1972), and the Rio San Juan Complex (Dominican Republic; 104 to 62 Ma; Krebs et al., 2008). In these cases, age disparities are associated with large differences in metamorphic grade including blueschists, eclogites, and amphibolites, although age variations do also occur among blocks of the same apparent metamorphic grade (see data compilation by Mulcahy et al. [2018]). In contrast, some mélange zones record no apparent differences in age among blocks, even when the blocks record resolvably different metamorphic histories. For example, age estimates on eclogites and amphibolitized blueschists from Sistan suture (Eastern Iran) based on $^{40}Ar/^{39}Ar$ white micas and hornblende ages are all ca. 86 Ma (Bonnet et al., 2018). This similarity was interpreted as representing coeval detachment and tectonic mixing during exhumation, as opposed to mixing during subduction as is the case with the Catalina Schist (see Bebout & Barton, 2002; Penniston-Dorland et al., 2014). In all of the localities, large disparities in either metamorphic age or history have been attributed to large-scale mixing of tectonic blocks within a deforming matrix (see Bonnet et al., 2018; Cloos, 1982; Gerya et al., 2002; Krebs et al., 2008).

Blocks from the amphibolite-facies mélange zone record a relatively narrow range of both peak metamorphic temperatures, from ~643 to 735°C (K. M. Harvey et al., 2021; Penniston-Dorland et al., 2018), and peak metamorphic ages, from ca. 116 to 108 Ma. The small, but resolvable, differences in peak metamorphic temperatures can be explained by limited mixing during crystallization of rheologically stiff mélange matrix phases including anthophyllite and enstatite (Penniston-Dorland et al., 2018). Two mechanisms could potentially explain both the limited spatial scale of mixing and the narrow range of ages recorded by the unit. The first is that mixing largely ceased following development of chain silicates in the matrix. Jamming of mélange at the subduction interface has been predicted to greatly reduce ductile deformation, resulting in episodic brittle deformation events similar to those observed during episodic tremor and slip (Beall et al., 2019; Webber et al., 2018). This mechanism is consistent with the observed spatial and temporal scales of mixing, as well as with field observations. The second possibility is that both of the amphibolite-facies units were underplated, causing localized deformation to cease as a new subduction interface developed beneath the two units. This mechanism has been proposed in other exhumed terranes that preserve progressively older metamorphic ages toward the top of the sequence (Angiboust et al., 2014). Underplating best explains the overall structural relationship between the combined amphibolite-facies units and the lower grade units, which occur in an inverted metamorphic stack (see Figure 1b) that becomes progressively younger structurally downward (Grove et al., 2008). Underplating also provides a mechanism for the limited spatial and temporal timescales of mixing recorded by the amphibolite-facies mélange zone if the duration between initial mélange formation and underplating was short. Given that rheologic changes at the subduction interface have been specifically proposed to cause underplating (Agard et al., 2009), these two mechanisms could have acted in concert.

$^{40}Ar/^{39}Ar$ white mica and Sm-Nd garnet ages from the amphibolite-units facies units favor differential cooling following underplating. Differences in white mica ages between the two units suggest that the coherent amphibolite cooled first, reaching ~400–450°C (Harrison et al., 2009) between 106 and 101 Ma. Assuming that the unit reached peak conditions of 690°C at or after ca. 115 Ma (Anczkiewicz et al., 2004; K. M. Harvey et al., 2021), these ages suggest that it cooled at a minimum rate between 18 and 28°C/Myr. In contrast, $^{40}Ar/^{39}Ar$ white mica ages from the amphibolite-facies mélange zone are younger and range from 101 to 97 Ma (Grove & Bebout, 1995). Predicted cooling rates based on peak Sm-Nd garnet ages for individual blocks (111.1–115.5 Ma) and corresponding Zr-in-rutile temperatures (643–721°C; Penniston-Dorland et al., 2018; see Table 1) are on average 22°C/Myr and range from 14 to 43°C/Myr. Collectively these observations suggest that the units cooled at similar rates yet asynchronously, with the lower coherent unit cooling earlier than the overriding mélange zone. Combined with the correlation between metamorphic

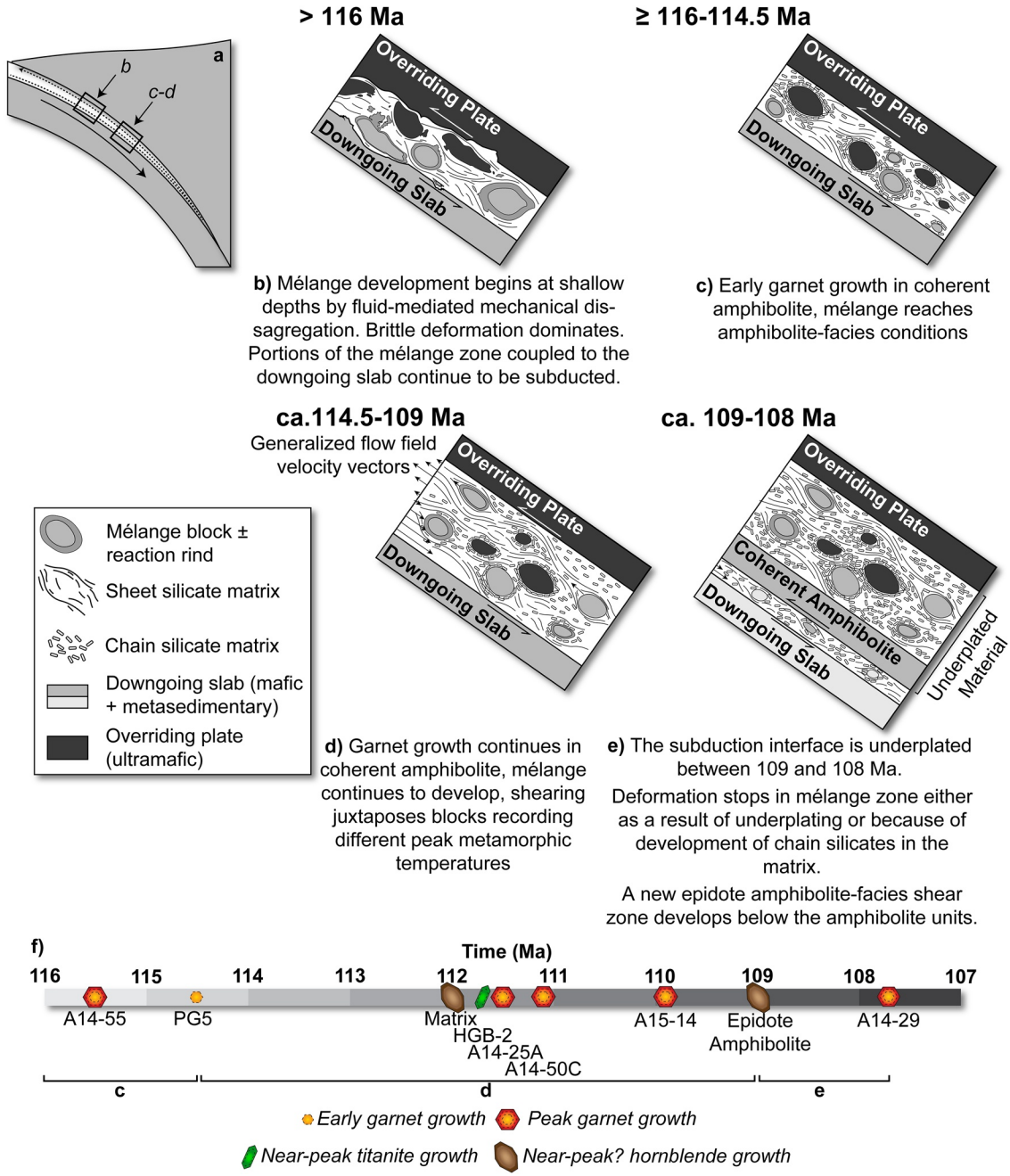

Figure 5. (a) Sketch of subduction zone interface showing narrowing of interface at depth and resultant return flow. (b–e) Proposed model for the development of the amphibolite-facies mélange zone of the Catalina Schist showing the evolution of the shear zone from early development at shallow depths prior to ca. 116 Ma to underplating and cooling between ca. 109 and 108 Ma. (e) Timeline summarizing key chronologic constraints on amphibolite-facies metamorphism relative to the proposed model. Other data sources: Anczkiewicz et al. (2004), Grove (1993), Grove and Bebout (1995), and Mattinson (1986).

grade and structural position of the different tectonometamorphic slices of the Catalina Schist (amphibolite facies at the top grading downwards into blueschist facies), the gradational bottom-to-top cooling recorded by the amphibolite units is consistent with refrigeration of the subduction interface as a result of isolation from the mantle wedge following underplating.

We propose the following scenario, shown as a conceptual model in Figure 5, to explain both the temperature and age variations among mélange zone blocks and the coherent amphibolite unit. (a) *The mélange zone and underlying coherent amphibolite reach amphibolite-facies conditions at or before ca. 116 Ma*. Mélange

formation occurs throughout prograde metamorphism as blocks are sourced from both the downgoing slab and overriding plate by fluid-mediated mechanical disaggregation (e.g., Penniston-Dorland et al., 2014). This stage corresponds to early garnet growth in the coherent portion of the subducting slab (Anczkiewicz et al., 2004). (b) *Between ca. 116 and 108 Ma, return flow resulting from narrowing of the subduction interface at depth* (Figure 5d) *in conjunction with shearing between mélange components juxtaposes blocks with different peak metamorphic conditions and ages*. This mixing results in non-systematic temperature variations observed among blocks throughout the unit (Penniston-Dorland et al., 2018) and corresponds with partial geochemical and isotopic homogenization of the matrix (e.g., Bebout & Barton, 2002; King et al., 2006, 2007) and metasomatism and mechanical ablation of the blocks (e.g., Penniston-Dorland et al., 2012, 2014; Sorensen & Barton, 1987; Sorensen & Grossman, 1989) (c) *The mélange zone and coherent amphibolite unit are both underplated between 109 Ma (the first record of metamorphism in the epidote amphibolite-facies unit) and 108 Ma (the last record of high-grade metamorphism in the two amphibolite-facies units)*. Underplating may be catalyzed by changes in the rheology of the mélange matrix, where crystallization of amphiboles and pyroxenes strengthen the matrix. A new shear zone develops between the downgoing slab and underplated material. (d) *The subduction interface is thermally isolated from the mantle wedge by the underplated material resulting in gradational cooling of the amphibolite-facies units*. Progressive underplating and cooling leads to the formation of the epidote amphibolite (ca. 109 Ma; Grove, 1993), epidote blueschist (ca. 98 Ma; Grove & Bebout, 1995) and lawsonite blueschist (ca. 98 Ma; Grove & Bebout, 1995) units.

6. Conclusions

The Catalina Schist is famous for its spectacular preservation of mélange zones at various structural positions and metamorphic grades. The amphibolite-facies mélange zone in particular has been utilized by a number of previous studies to understand mass transport, metasomatism, melt generation and tectonic mixing at the subduction interface (e.g., Barnes et al., 2019; Bebout, 1997; Bebout & Barton, 1989, 1993, 2002; King et al., 2006, 2007; Page et al., 2019; Penniston-Dorland et al., 2014, 2018; Sorensen & Barton, 1987; Sorensen & Grossman, 1989). New Sm-Nd garnet ages for blocks from the amphibolite-facies mélange zone reveal that the mélange zone developed at amphibolite-facies conditions over at least 7.8 ± 6.3 Myr from ≥115.5 ± 3.0 to 107.7 ± 5.5 Ma, which is rapid compared to age disparities as large as 40 million years recorded within other tectonic mélange zones (e.g., Krebs et al., 2008; Mulcahy et al., 2018). During this time, progressive tectonic mixing via mélange flow in conjunction with shearing between matrix components juxtaposed blocks from different depths. The ~90°C variation in peak metamorphic temperature recorded by blocks throughout the mélange zone suggests that the scale of mixing was limited (K. M. Harvey et al., 2021; Penniston-Dorland et al., 2018). Previous studies attributed this limited scale of mixing to rheologically stiff matrix phases which inhibited differential movement of blocks (Penniston-Dorland et al., 2018). These new ages show that the mélange zone developed at amphibolite-facies conditions relatively quickly, which likely also contributed to the small scale of mixing observed. The mélange zone appears to have been underplated between 109 and 108 Ma, resulting in down-stepping of the subduction interface and formation of the underlying epidote amphibolite-facies unit. Underplating caused deformation and therefore mixing within the amphibolite-facies zone to cease, as the unit cooled at rates between 14 and 43°C/Myr from amphibolite facies conditions to <400–425°C between 106 and 101 Ma.

Data Availability Statement

Supporting Information S1 for this manuscript are archived in the University of Maryland's Digital Repository (DRUM) and are available at https://doi.org/10.13016/v3n5-2lxc.

Acknowledgments
This work was funded by NSF grants EAR-1419871 (to S. C. Penniston-Dorland) and EAR-1419865 (to M. J. Kohn) with additional support from EAR-1850786 to S. C. Penniston-Dorland and the Geological Society of America's Graduate Student Research Grant (2018, 2019) to K. M. Harvey. Laboratory work was supported in part by the Center for Isotope Geochemistry at Boston College. P. G. Starr and M. J. Kohn gratefully acknowledge funding from NSF grant OIA-1545903 (to M. J. Kohn, S. C. Penniston-Dorland, and M. Feineman). The authors thank Phil Piccoli (UMD) for his assistance with EPMA analyses, Richard Ash (UMD) for assistance with LA-ICP-MS analyses and Mike Tappa for assistance with TIMS analyses at Boston College. The authors acknowledge the support of the Maryland NanoCenter and its AIMLab as well as the Plasma Lab housed in the University of Maryland Department of Geology. The authors also gratefully thank Noah McLean (University of Kansas) for insightful discussion about statistics in geochronology. The manuscript greatly benefitted from thoughtful and constructive reviews by Miguel Cisneros and Sean Mulcahy as well as editorial handling by Whitney Behr. Finally, the authors thank the Santa Catalina Island Conservancy for support with sample collection of the Catalina Schist.

References

Abratis, M., & Wörner, G. (2001). Ridge collision, slab-window formation, and the flux of Pacific asthenosphere into the Caribbean realm. *Geology*, *29*(2), 127–130. https://doi.org/10.1130/0091-7613(2001)029<0127:rcswfa>2.0.co;2

Agard, P., Plunder, A., Angiboust, S., Bonnet, G., & Ruh, J. (2018). The subduction plate interface: Rock record and mechanical coupling (from long to short timescales). *Lithos*, *320–321*, 537–566. https://doi.org/10.1016/j.lithos.2018.09.029

Agard, P., Yamato, P., Jolivet, L., & Burov, E. (2009). Exhumation of oceanic blueschists and eclogites in subduction zones: Timing and mechanisms. *Earth-Science Reviews*, *92*(1–2), 53–79. https://doi.org/10.1016/j.earscirev.2008.11.002

Anczkiewicz, R., Platt, J. P., Thirlwall, M. F., & Wakabayashi, J. (2004). Franciscan subduction off to a slow start: Evidence from high-precision Lu–Hf garnet ages on high grade-blocks. *Earth and Planetary Science Letters*, *225*(1–2), 147–161. https://doi.org/10.1016/j.epsl.2004.06.003

Angiboust, S., Glodny, J., Oncken, O., & Chopin, C. (2014). In search of transient subduction interfaces in the Dent Blanche–Sesia Tectonic System (W. Alps). *Lithos*, *205*, 298–321. https://doi.org/10.1016/j.lithos.2014.07.001

Armstrong, J. T. (1988). Quantitative analysis of silicate and oxide minerals: Comparison of Monte Carlo, ZAF and phi-rho-z procedures. In D. E. Newbury (Ed.), *Microbeam analysis* (pp. 239–246). San Francisco Press.

Audet, P., & Bürgmann, R. (2014). Possible control of subduction zone slow-earthquake periodicity by silica enrichment. *Nature*, *510*(7505), 389–392. https://doi.org/10.1038/nature13391

Baldwin, S. L., Harrison, T. M., & Gerald, J. D. F. (1990). Diffusion of ^{40}Ar in metamorphic hornblende. *Contributions to Mineralogy and Petrology*, *105*(6), 691–703. https://doi.org/10.1007/BF00306534

Barnes, J. D., Penniston-Dorland, S. C., Bebout, G. E., Hoover, W., Beaudoin, G. M., & Agard, P. (2019). Chlorine and lithium behavior in metasedimentary rocks during prograde metamorphism: A comparative study of exhumed subduction complexes (Catalina Schist and Schistes Lustrés). *Lithos*, *336–337*, 40–53. https://doi.org/10.1016/j.lithos.2019.03.028

Baxter, E. F., Ague, J. J., & Depaolo, D. J. (2002). Prograde temperature–time evolution in the Barrovian type–locality constrained by Sm/Nd garnet ages from Glen Clova, Scotland. *Journal of the Geological Society*, *159*(1), 71–82. https://doi.org/10.1144/0016-76901013

Baxter, E. F., Caddick, M. J., & Dragovic, B. (2017). Garnet: A rock-forming mineral petrochronometer. *Reviews in Mineralogy and Geochemistry*, *83*(1), 469–533. https://doi.org/10.2138/rmg.2017.83.15

Baxter, E. F., & Scherer, E. E. (2013). Garnet geochronology: Timekeeper of tectonometamorphic processes. *Elements*, *9*(6), 433–438. https://doi.org/10.2113/gselements.9.6.433

Beall, A., Fagereng, Å., & Ellis, S. (2019). Strength of strained two-phase mixtures: Application to rapid creep and stress amplification in subduction zone mélange. *Geophysical Research Letters*, *46*(1), 169–178. https://doi.org/10.1029/2018GL081252

Bebout, G. E. (1997). Nitrogen isotope tracers of high-temperature fluid-rock interactions: Case study of the Catalina Schist, California. *Earth and Planetary Science Letters*, *151*(1–2), 77–90. https://doi.org/10.1016/S0012-821X(97)00117-9

Bebout, G. E., & Barton, M. D. (1989). Fluid flow and metasomatism in a subduction zone hydrothermal system: Catalina Schist terrane, California. *Geology*, *17*(11), 976–980. https://doi.org/10.1130/0091-7613(1989)017<0976:ffamia>2.3.co;2

Bebout, G. E., & Barton, M. D. (1993). Metasomatism during subduction: Products and possible paths in the Catalina Schist, California. *Chemical Geology*, *108*, 61–92. https://doi.org/10.1016/0009-2541(93)90318-D

Bebout, G. E., & Barton, M. D. (2002). Tectonic and metasomatic mixing in a high-T, subduction-zone mélange—Insights into the geochemical evolution of the slab–mantle interface. *Chemical Geology*, *187*(1–2), 79–106. https://doi.org/10.1016/S0009-2541(02)00019-0

Bebout, G. E., & Penniston-Dorland, S. C. (2016). Fluid and mass transfer at subduction interfaces—The field metamorphic record. *Lithos*, *240–243*, 228–258. https://doi.org/10.1016/j.lithos.2015.10.007

Behr, W. M., & Bürgmann, R. (2021). What's down there? The structures, materials and environment of deep-seated slow slip and tremor. *Philosophical Transactions of the Royal Society A: Mathematical, Physical and Engineering Sciences*, *379*(2193), 20200218. https://doi.org/10.1098/rsta.2020.0218

Bloch, E., & Ganguly, J. (2015). ^{176}Lu–^{176}Hf geochronology of garnet II: Numerical simulations of the development of garnet–whole-rock ^{176}Lu–^{176}Hf isochrons and a new method for constraining the thermal history of metamorphic rocks. *Contributions to Mineralogy and Petrology*, *169*(2), 14. https://doi.org/10.1007/s00410-015-1115-x

Bloch, E., Ganguly, J., Hervig, R., & Cheng, W. (2015). ^{176}Lu–^{176}Hf geochronology of garnet I: Experimental determination of the diffusion kinetics of Lu^{3+} and Hf^{4+} in garnet, closure temperatures and geochronological implications. *Contributions to Mineralogy and Petrology*, *169*(2), 12. https://doi.org/10.1007/s00410-015-1109-8

Bloch, E. M., Jollands, M. C., Devoir, A., Bouvier, A.-S., Ibañez-Mejia, M., & Baumgartner, L. P. (2020). Multispecies diffusion of yttrium, rare earth elements and hafnium in garnet. *Journal of Petrology*, *61*(7). https://doi.org/10.1093/petrology/egaa055

Bonnet, G., Agard, P., Angiboust, S., Monié, P., Jentzer, M., Omrani, J., et al. (2018). Tectonic slicing and mixing processes along the subduction interface: The Sistan example (Eastern Iran). *Lithos*, *310–311*, 269–287. https://doi.org/10.1016/j.lithos.2018.04.016

Carlson, W. D. (2006). Rates of Fe, Mg, Mn, and Ca diffusion in garnet. *American Mineralogist*, *91*(1), 1–11. https://doi.org/10.2138/am.2006.2043

Carlson, W. D. (2012). Rates and mechanism of Y, REE, and Cr diffusion in garnet. *American Mineralogist*, *97*(10), 1598–1618. https://doi.org/10.2138/am.2012.4108

Catlos, E. J., & Sorensen, S. S. (2003). Phengite-based chronology of K- and Ba-rich fluid flow in two paleosubduction zones. *Science*, *299*(5603), 92–95. https://doi.org/10.1126/science.1076977

Chakraborty, S., & Ganguly, J. (1992). Cation diffusion in aluminosilicate garnets: Experimental determination in spessartine-almandine diffusion couples, evaluation of effective binary diffusion coefficients, and applications. *Contributions to Mineralogy and Petrology*, *111*(1), 74–86. https://doi.org/10.1007/BF00296579

Cheng, H., DuFrane, S. A., Vervoort, J. D., Nakamura, E., Zheng, Y.-F., & Zhou, Z. (2010). Protracted oceanic subduction prior to continental subduction: New Lu-Hf and Sm-Nd geochronology of oceanic-type high-pressure eclogite in the western Dabie orogen. *American Mineralogist*, *95*(8–9), 1214–1223. https://doi.org/10.2138/am.2010.3307

Cheng, H., King, R. L., Nakamura, E., Vervoort, J. D., & Zhou, Z. (2008). Coupled Lu-Hf and Sm-Nd geochronology constrains garnet growth in ultra-high-pressure eclogites from the Dabie orogen. *Journal of Metamorphic Geology*, *26*(7), 741–758. https://doi.org/10.1111/j.1525-1314.2008.00785.x

Cheng, H., Vervoort, J. D., Dragovic, B., Wilford, D., & Zhang, L. (2018). Coupled Lu–Hf and Sm–Nd geochronology on a single eclogitic garnet from the Huwan shear zone, China. *Chemical Geology*, *476*, 208–222. https://doi.org/10.1016/j.chemgeo.2017.11.018

Cloos, M. (1982). Flow melanges: Numerical modeling and geologic constraints on their origin in the Franciscan subduction complex, California. *Geological Society of America Bulletin*, *93*(4), 330–345. https://doi.org/10.1130/0016-7606(1982)93<330:fmnmag>2.0.co;2

DeLong, S. E., Schwarz, W. M., & Anderson, R. N. (1979). Thermal effects of ridge subduction. *Earth and Planetary Science Letters*, *44*(2), 239–246. https://doi.org/10.1016/0012-821X(79)90172-9

Dragovic, B., Angiboust, S., & Tappa, M. J. (2020). Petrochronological close-up on the thermal structure of a paleo-subduction zone (W. Alps). *Earth and Planetary Science Letters*, *547*, 116446. https://doi.org/10.1016/j.epsl.2020.116446

Dragovic, B., Baxter, E. F., & Caddick, M. J. (2015). Pulsed dehydration and garnet growth during subduction revealed by zoned garnet geochronology and thermodynamic modeling, Sifnos, Greece. *Earth and Planetary Science Letters*, *413*, 111–122. https://doi.org/10.1016/j.epsl.2014.12.024

Dragovic, B., Samanta, L. M., Baxter, E. F., & Selverstone, J. (2012). Using garnet to constrain the duration and rate of water-releasing metamorphic reactions during subduction: An example from Sifnos, Greece. *Chemical Geology*, *314–317*, 9–22. https://doi.org/10.1016/j.chemgeo.2012.04.016

Firsov, L. V., & Dobretsov, N. L. (1970). Age of glaucophane metamorphism at the northwestern fringe of the Pacific Ocean. *Doklady Akademii Nauk SSSR*, *185*, 46–48.

French, M. E., & Zhu, W. (2017). Slow fault propagation in serpentinite under conditions of high pore fluid pressure. *Earth and Planetary Science Letters*, *473*, 131–140. https://doi.org/10.1016/j.epsl.2017.06.009

Gerya, T. V., Stöckhert, B., & Perchuk, A. L. (2002). Exhumation of high-pressure metamorphic rocks in a subduction channel: A numerical simulation. *Tectonics*, *21*(6), 6-1–6-19. https://doi.org/10.1029/2002TC001406

Grove, M. (1993). *Thermal histories of southern California basement terranes* (Ph.D. Thesis). University of California.

Grove, M., & Bebout, G. E. (1995). Cretaceous tectonic evolution of coastal southern California: Insights from the Catalina Schist. *Tectonics*, *14*(6), 1290–1308. https://doi.org/10.1029/95tc01931

Grove, M., Bebout, G. E., Jacobson, C. E., Barth, A. P., Kimbrough, D. L., King, R. L., et al. (2008). The Catalina Schist: Evidence for middle Cretaceous subduction erosion of southwestern North America. *Special Paper 436: Formation and Applications of the Sedimentary Record in Arc Collision Zones*, *436*, 335–361. https://doi.org/10.1130/2008.2436(15)

Harrison, T. M., Célérier, J., Aikman, A. B., Hermann, J., & Heizler, M. T. (2009). Diffusion of ^{40}Ar in muscovite. *Geochimica et Cosmochimica Acta*, *73*(4), 1039–1051. https://doi.org/10.1016/j.gca.2008.09.038

Harvey, J., & Baxter, E. F. (2009). An improved method for TIMS high precision neodymium isotope analysis of very small aliquots (1–10 ng). *Chemical Geology*, *258*(3–4), 251–257. https://doi.org/10.1016/j.chemgeo.2008.10.024

Harvey, K. M., Penniston-Dorland, S. C., Kohn, M. J., & Piccoli, P. M. (2021). Assessing P-T variability in mélange blocks from the Catalina Schist: Is there differential movement at the subduction interface? *Journal of Metamorphic Geology*, *39*(3), 271–295. https://doi.org/10.1111/jmg.12571

Hickmott, D., & Spear, F. S. (1992). Major-and trace-element zoning in garnets from calcareous pelites in the NW Shelburne Falls Quadrangle, Massachusetts: Garnet growth histories in retrograded rocks. *Journal of Petrology*, *33*(5), 965–1005. https://doi.org/10.1093/petrology/33.5.965

Hickmott, D. D., Shimizu, N., Spear, F. S., & Selverstone, J. (1987). Trace-element zoning in a metamorphic garnet. *Geology*, *15*(6), 573–576. https://doi.org/10.1130/0091-7613(1987)15<573:tziamg>2.0.co;2

Hollister, L. S. (1966). Garnet zoning: An interpretation based on the Rayleigh fractionation model. *Science*, *154*(3757), 1647–1651. https://doi.org/10.1126/science.154.3757.1647

Ishizuka, O., Tani, K., Reagan, M. K., Kanayama, K., Umino, S., Harigane, Y., et al. (2011). The timescales of subduction initiation and subsequent evolution of an oceanic island arc. *Earth and Planetary Science Letters*, *306*(3–4), 229–240. https://doi.org/10.1016/j.epsl.2011.04.006

Iwamori, H. (2000). Thermal effects of ridge subduction and its implications for the origin of granitic batholith and paired metamorphic belts. *Earth and Planetary Science Letters*, *181*(1–2), 131–144. https://doi.org/10.1016/S0012-821X(00)00182-5

Jochum, K. P., Weis, U., Stoll, B., Kuzmin, D., Yang, Q., Raczek, I., et al. (2011). Determination of reference values for NIST SRM 610-617 glasses following ISO guidelines. *Geostandards and Geoanalytical Research*, *35*(4), 397–429. https://doi.org/10.1111/j.1751-908X.2011.00120.x

Jochum, K. P., Willbold, M., Raczek, I., Stoll, B., & Herwig, K. (2005). Chemical characterisation of the USGS reference glasses GSA-1G, GSC-1G, GSD-1G, GSE-1G, BCR-2G, BHVO-2G and BIR-1G using EPMA, ID-TIMS, ID-ICP-MS and LA-ICP-MS. *Geostandards and Geoanalytical Research*, *29*(3), 285–302. https://doi.org/10.1111/j.1751-908X.2005.tb00901.x

King, R. L., Bebout, G., Moriguti, T., & Nakamura, E. (2006). Elemental mixing systematics and Sr–Nd isotope geochemistry of mélange formation: Obstacles to identification of fluid sources to arc volcanics. *Earth and Planetary Science Letters*, *246*(3–4), 288–304. https://doi.org/10.1016/j.epsl.2006.03.053

King, R. L., Bebout, G. E., Grove, M., Moriguti, T., & Nakamura, E. (2007). Boron and lead isotope signatures of subduction-zone mélange formation: Hybridization and fractionation along the slab–mantle interface beneath volcanic arcs. *Chemical Geology*, *239*(3–4), 305–322. https://doi.org/10.1016/j.chemgeo.2007.01.009

Kirkpatrick, J. D., Fagereng, Å., & Shelly, D. R. (2021). Geological constraints on the mechanisms of slow earthquakes. *Nature Reviews Earth & Environment*, *2*(4), 285–301. https://doi.org/10.1038/s43017-021-00148-w

Kohn, M. J. (2009). Models of garnet differential geochronology. *Geochimica et Cosmochimica Acta*, *73*(1), 170–182. https://doi.org/10.1016/j.gca.2008.10.004

Kohn, M. J. (2020). A refined zirconium-in-rutile thermometer. *American Mineralogist*, *105*, 963–971. https://doi.org/10.2138/am-2020-7091

Kohn, M. J., Corrie, S. L., & Markley, C. (2015). The fall and rise of metamorphic zircon. *American Mineralogist*, *100*(4), 897–908. https://doi.org/10.2138/am-2015-5064

Krebs, M., Maresch, W. V., Schertl, H.-P., Münker, C., Baumann, A., Draper, G., et al. (2008). The dynamics of intra-oceanic subduction zones: A direct comparison between fossil petrological evidence (Rio San Juan Complex, Dominican Republic) and numerical simulation. *Lithos*, *103*(1–2), 106–137. https://doi.org/10.1016/j.lithos.2007.09.003

Krebs, M., Schertl, H.-P., Maresch, W. V., & Draper, G. (2011). Mass flow in serpentinite-hosted subduction channels: *P–T–t* path patterns of metamorphic blocks in the Rio San Juan mélange (Dominican Republic). *Journal of Asian Earth Sciences*, *42*(4), 569–595. https://doi.org/10.1016/j.jseaes.2011.01.011

Krohe, A. (2017). The Franciscan Complex (California, USA) – The model case for return-flow in a subduction channel put to the test. *Gondwana Research*, *45*, 282–307. https://doi.org/10.1016/j.gr.2017.02.003

Kylander-Clark, A. R. C., Hacker, B. R., Johnson, C. M., Beard, B. L., Mahlen, N. J., & Lapen, T. J. (2007). Coupled Lu–Hf and Sm–Nd geochronology constrains prograde and exhumation histories of high- and ultrahigh-pressure eclogites from western Norway. *Chemical Geology*, *242*(1–2), 137–154. https://doi.org/10.1016/j.chemgeo.2007.03.006

Lapen, T. J., Johnson, C. M., Baumgartner, L. P., Mahlen, N. J., Beard, B. L., & Amato, J. M. (2003). Burial rates during prograde metamorphism of an ultra-high-pressure terrane: An example from Lago di Cignana, western Alps, Italy. *Earth and Planetary Science Letters*, *215*(1–2), 57–72. https://doi.org/10.1016/S0012-821X(03)00455-2

Lister, G. S., & Baldwin, S. L. (1996). Modelling the effect of arbitrary *P-T-t* histories on argon diffusion in minerals using the MacArgon program for the Apple Macintosh. *Tectonophysics*, *253*(1–2), 83–109. https://doi.org/10.1016/0040-1951(95)00059-3

Mattinson, J. M. (1986). Geochronology of high-pressure–low-temperature Franciscan metabasites: A new approach using the U-Pb system. In Blueschists and eclogites (Vol. 164, pp. 95–106). Geological Society of America. https://doi.org/10.1130/MEM164-p95

Menant, A., Sternai, P., Jolivet, L., Guillou-Frottier, L., & Gerya, T. (2016). 3D numerical modeling of mantle flow, crustal dynamics and magma genesis associated with slab roll-back and tearing: The eastern Mediterranean case. *Earth and Planetary Science Letters*, *442*, 93–107. https://doi.org/10.1016/j.epsl.2016.03.002

Morton, D. M., Miller, F. K., Kistler, R. W., Premo, W. R., Lee, C.-T. A., Langenheim, V. E., et al. (2014). Framework and petrogenesis of the northern Peninsular Ranges batholith, southern California. In D. M. Morton & F. K. Miller (Eds.), *Peninsular Ranges Batholith, Baja California and Southern California*. Geological Society of America. https://doi.org/10.1130/2014.1211(03)

Mulcahy, S. R., Starnes, J. K., Day, H. W., Coble, M. A., & Vervoort, J. D. (2018). Early Onset of Franciscan Subduction. *Tectonics*, *37*(5), 1194–1209. https://doi.org/10.1029/2017TC004753

Page, F. Z., Cameron, E. M., Flood, C. M., Dobbins, J. W., Spicuzza, M. J., Kitajima, K., et al. (2019). Extreme oxygen isotope zoning in garnet and zircon from a metachert block in mélange reveals metasomatism at the peak of subduction metamorphism. *Geology*, *47*(7), 655–658. https://doi.org/10.1130/G46135.1

Paton, C., Hellstrom, J., Paul, B., Woodhead, J., & Hergt, J. (2011). Iolite: Freeware for the visualisation and processing of mass spectrometric data. *Journal of Analytical Atomic Spectrometry*, *26*(12), 2508. https://doi.org/10.1039/c1ja10172b

Peacock, S. M. (1991). Numerical simulation of subduction zone pressure-temperature-time paths: Constraints on fluid production and arc magmatism. *Philosophical Transactions of the Royal Society of London. Series A: Physical and Engineering Sciences*, *335*(1638), 341–353. https://doi.org/10.1098/rsta.1991.0050

Peacock, S. M. (1996). Thermal and petrologic structure of subduction zones. In G. E. Bebout, D. W. Scholl, S. H. Kirby, & J. P. Platt (Eds.), *Subduction* (pp. 119–133). https://doi.org/10.1029/GM096p0119

Penniston-Dorland, S. C., Bebout, G. E., Pogge von Strandmann, P. A. E., Elliott, T., & Sorensen, S. S. (2012). Lithium and its isotopes as tracers of subduction zone fluids and metasomatic processes: Evidence from the Catalina Schist, California, USA. *Geochimica et Cosmochimica Acta*, *77*, 530–545. https://doi.org/10.1016/j.gca.2011.10.038

Penniston-Dorland, S. C., Gorman, J. K., Bebout, G. E., Piccoli, P. M., & Walker, R. J. (2014). Reaction rind formation in the Catalina Schist: Deciphering a history of mechanical mixing and metasomatic alteration. *Chemical Geology*, *384*, 47–61. https://doi.org/10.1016/j.chemgeo.2014.06.024

Penniston-Dorland, S. C., Kohn, M. J., & Manning, C. E. (2015). The global range of subduction zone thermal structures from exhumed blueschists and eclogites: Rocks are hotter than models. *Earth and Planetary Science Letters*, *428*, 243–254. https://doi.org/10.1016/j.epsl.2015.07.031

Penniston-Dorland, S. C., Kohn, M. J., & Piccoli, P. M. (2018). A mélange of subduction temperatures: Evidence from Zr-in-rutile thermometry for strengthening of the subduction interface. *Earth and Planetary Science Letters*, *482*, 525–535. https://doi.org/10.1016/j.epsl.2017.11.005

Platt, J. (1975). Metamorphic and deformational processes in the Franciscan Complex, California: Some insights from the Catalina Schist terrane. *Geological Society of America Bulletin*, *86*(10), 1337–1347. https://doi.org/10.1130/0016-7606(1975)86<1337:madpit>2.0.co;2

Platt, J. (1976). *The significance of the Catalina Schist in the history of the southern California borderland* (Ph.D. Thesis). University of California.

Plunder, A., Agard, P., Chopin, C., Pourteau, A., & Okay, A. I. (2015). Accretion, underplating and exhumation along a subduction interface: From subduction initiation to continental subduction (Tavşanlı zone, W. Turkey). *Lithos*, *226*, 233–254. https://doi.org/10.1016/j.lithos.2015.01.007

Pollington, A. D., & Baxter, E. F. (2011). High precision microsampling and preparation of zoned garnet porphyroblasts for Sm–Nd geochronology. *Chemical Geology*, *281*(3–4), 270–282. https://doi.org/10.1016/j.chemgeo.2010.12.014

Santosh, M., & Kusky, T. (2010). Origin of paired high pressure–ultrahigh-temperature orogens: A ridge subduction and slab window model. *Terra Nova*, *22*(1), 35–42. https://doi.org/10.1111/j.1365-3121.2009.00914.x

Scherer, E. E., Cameron, K. L., & Blichert-Toft, J. (2000). Lu–Hf garnet geochronology: Closure temperature relative to the Sm–Nd system and the effects of trace mineral inclusions. *Geochimica et Cosmochimica Acta*, *64*(19), 3413–3432. https://doi.org/10.1016/S0016-7037(00)00440-3

Shaw, S. E., Todd, V. R., & Grove, M. (2003). Jurassic peraluminous gneissic granites in the axial zone of the Peninsular Ranges, southern California. In S. E. Johnson, S. R. Paterson, J. M. Fletcher, G. H. Girty, D. L. Kimbrough, & A. Martín-Barajas (Eds.), *Tectonic evolution of northwestern Mexico and the Southwestern USA*. Geological Society of America. https://doi.org/10.1130/0-8137-2374-4.157

Skora, S., Baumgartner, L. P., Mahlen, N. J., Johnson, C. M., Pilet, S., & Hellebrand, E. (2006). Diffusion-limited REE uptake by eclogite garnets and its consequences for Lu–Hf and Sm–Nd geochronology. *Contributions to Mineralogy and Petrology*, *152*(6), 703–720. https://doi.org/10.1007/s00410-006-0128-x

Smit, M. A., Scherer, E. E., & Mezger, K. (2013). Lu–Hf and Sm–Nd garnet geochronology: Chronometric closure and implications for dating petrological processes. *Earth and Planetary Science Letters*, *381*, 222–233. https://doi.org/10.1016/j.epsl.2013.08.046

Sorensen, S. S. (1984). *Petrology of basement rocks of the California Continental Borderland and the Los Angeles Basin* (Ph.D. Thesis). University of California.

Sorensen, S. S. (1988). Petrology of amphibolite-facies mafic and ultramafic rocks from the Catalina Schist, southern California: Metasomatism and migmatization in a subduction zone metamorphic setting. *Journal of Metamorphic Geology*, *6*(4), 405–435. https://doi.org/10.1111/j.1525-1314.1988.tb00431.x

Sorensen, S. S., & Barton, M. D. (1987). Metasomatism and partial melting in a subduction complex Catalina Schist, southern California. *Geology*, *15*(2), 115–118. https://doi.org/10.1130/0091-7613(1987)15<115:mapmia>2.0.co;2

Sorensen, S. S., & Grossman, J. (1989). Enrichment of trace elements in garnet amphibolites from a paleo-subduction zone: Catalina Schist, southern California. *Geochimica et Cosmochimica Acta*, *53*(12), 3155–3177. https://doi.org/10.1016/0016-7037(89)90096-3

Spinelli, G. A., & Harris, R. N. (2011). Thermal effects of hydrothermal circulation and seamount subduction: Temperatures in the Nankai Trough Seismogenic Zone Experiment transect, Japan. *Geochemistry, Geophysics, Geosystems*, *12*(12). https://doi.org/10.1029/2011GC003727

Starr, P. G., Broadwell, K. S., Dragovic, B., Scambelluri, M., Haws, A. A., Caddick, M. J., et al. (2020). The subduction and exhumation history of the Voltri Ophiolite, Italy: Evaluating exhumation mechanisms for high-pressure metamorphic massifs. *Lithos*, *376–377*, 105767. https://doi.org/10.1016/j.lithos.2020.105767

Suppe, J., & Armstrong, R. L. (1972). Potassium-argon dating of Franciscan metamorphic rocks. *American Journal of Science*, *272*(3), 217–233. https://doi.org/10.2475/ajs.272.3.217

Tarling, M. S., Smith, S. A. F., & Scott, J. M. (2019). Fluid overpressure from chemical reactions in serpentinite within the source region of deep episodic tremor. *Nature Geoscience*, *12*(12), 1034–1042. https://doi.org/10.1038/s41561-019-0470-z

Thöni, M. (2002). Sm–Nd isotope systematics in garnet from different lithologies (Eastern Alps): Age results, and an evaluation of potential problems for garnet Sm–Nd chronometry. *Chemical Geology*, *185*(3–4), 255–281. https://doi.org/10.1016/S0009-2541(01)00410-7

Thorkelson, D. J., Madsen, J. K., & Sluggett, C. L. (2011). Mantle flow through the Northern Cordilleran slab window revealed by volcanic geochemistry. *Geology*, *39*(3), 267–270. https://doi.org/10.1130/G31522.1

Tirone, M., Ganguly, J., Dohmen, R., Langenhorst, F., Hervig, R., & Becker, H.-W. (2005). Rare earth diffusion kinetics in garnet: Experimental studies and applications. *Geochimica et Cosmochimica Acta*, *69*(9), 2385–2398. https://doi.org/10.1016/j.gca.2004.09.025

Tsujimori, T., Sisson, V. B., Liou, J. G., Harlow, G. E., & Sorensen, S. S. (2006). Petrologic characterization of Guatemalan lawsonite eclogite: Eclogitization of subducted oceanic crust in a cold subduction zone. In B. R. Hacker, W. C. McClelland, & J. G. Liou (Eds.), *Ultra-high-pressure metamorphism: Deep continental subduction*. Geological Society of America. https://doi.org/10.1130/2006.2403(09)

US Geological Survey. (2021). *The National Map: 3D Elevation Program [Map]*. Retrieved from https://apps.nationalmap.gov/viewer/

Vermeesch, P. (2018). IsoplotR: A free and open toolbox for geochronology. *Geoscience Frontiers*, *9*(5), 1479–1493. https://doi.org/10.1016/j.gsf.2018.04.001

Wakabayashi, J., & Dilek, Y. (2003). What constitutes 'emplacement' of an ophiolite?: Mechanisms and relationship to subduction initiation and formation of metamorphic soles. *Geological Society, London, Special Publications*, *218*(1), 427–447. https://doi.org/10.1144/GSL.SP.2003.218.01.22

Webber, S., Ellis, S., & Fagereng, Å. (2018). "Virtual shear box" experiments of stress and slip cycling within a subduction interface mélange. *Earth and Planetary Science Letters*, *488*, 27–35. https://doi.org/10.1016/j.epsl.2018.01.035

Whitney, D. L., & Evans, B. W. (2010). Abbreviations for names of rock-forming minerals. *American Mineralogist*, *95*(1), 185–187. https://doi.org/10.2138/am.2010.3371

Zack, T., Moraes, R., & Kronz, A. (2004). Temperature dependence of Zr in rutile: Empirical calibration of a rutile thermometer. *Contributions to Mineralogy and Petrology*, *148*(4), 471–488. https://doi.org/10.1007/s00410-004-0617-8